

---

SURFACE.  
THIN FILMS

---

# Atomic Force Microscopy Modified for Studying Electric Properties of Thin Films and Crystals. Review

K. L. Sorokina and A. L. Tolstikhina

*Shubnikov Institute of Crystallography, Russian Academy of Sciences,  
Leninskii pr. 59, Moscow, 119333 Russia*

*e-mail: sorokina@ns.crys.ras.ru*

Received June 19, 2003

**Abstract**—Probe force microscopy continues growing in popularity as a method for studying surfaces of solids and control over crystals and thin films that are grown on various scientific and industrial setups. New modifications of the method increase the possibilities for recording various characteristics of the objects studied. An important role here is played by “electrical” force microscopy, the various modifications and practical applications of which are considered below, as well as the results obtained by this method. © 2004 MAIK “Nauka/Interperiodica”.

## CONTENTS

### Introduction

1. From Imaging Surfaces to Precision Measurements
2. The Principle Underlying Measurements of Electric Parameters
3. Scanning Kelvin Probe Microscopy
4. Electrostatic Force Microscopy
5. Scanning Capacitance Microscopy

## INTRODUCTION

Since the construction of the first atomic force microscope [1], this new method of imaging surfaces has actively been used in various fields of research. The method itself is also rapidly developing and forms the basis for the development of a number of new scanning force techniques.

A microscope probe (elastic cantilever with a fine tip end), moving close to the sample surface, is under the action of various forces. Depending on the material of the probe (conducting or nonconducting, magnetic or nonmagnetic) and the tip–surface distance, these forces influence the probe motion to different extents. This fact is promising for point-to-point recording of the changes in the acting forces, with each of them containing some specific information on the properties of the object. The possibility of extracting the necessary information at each point of the object is provided by the unique system of probe motion with respect to a sample (a piezoelectric ceramic manipulator originally designed for a scanning tunneling microscope ensures the motion on a scale of thousandths of nanometer), the use of superminiaturized probes (100–400- $\mu\text{m}$ -long

cantilevers with about  $3 \times 30\text{-}\mu\text{m}$ -cross sections and 15–20- $\mu\text{m}$ -long tips with an apex diameter of about several nanometers) and the system of optical detection of cantilever deflection (sensitivity of the laser interferometers is of the order of  $10^{-5} \text{ nm Hz}^{-1/2}$ ).

## 1. FROM IMAGING SURFACES TO PRECISION MEASUREMENTS

The first similar images were obtained with the aid of “magnetic forces”—using a tip prepared from a magnetic material, Martin and Wickramasinghe [2] and Saénz *et al.* [3] managed to visualize the domain structure of surfaces [2, 3]. This gave an impetus to theoreticians for developing the theory of the new method [4–7]. Electrostatic forces also attracted the attention of researchers and, first and foremost, of experimenters [8–12]. This brings up the question whether it is possible to use various physical effects and measure locally defined parameters by scanning objects and, finally, obtain the distribution of thus measured physical quantities over the surface. Earlier, microscopists tried to extract information on surface relief from the data on the variation of a certain physical quantity along the surface (as in the first modification of a scanning capacitance microscope [13]). Now, it has become possible to measure a certain quantity and, at the same time, to study the surface topography. As a result, the precision methods for local determination of various physical parameters were developed on the basis of atomic force microscopy (AFM). These methods allowed one to compare the surface distributions of physical parameters with the observed morphological characteristics.

Today, the “magnetic images” mentioned above are studied by magnetic force microscopy [14]. We concentrate our attention on the study of only electric characteristics. We would like to stipulate that the quantities measured can have different degrees of locality, in other words, they can relate to surface regions having different areas. As will be shown later, the “locality” of the electrostatic potential set at each point of the space is determined by certain basic methodological restrictions. The contributions to the capacitance, a characteristic of the whole probe–sample system, come from all the regions of the surface, but these contributions decrease approximately inversely proportionally to the distance of the region from the point of the probe location [15]. The information contained in the differential capacitance (the change in the capacitance with the change in the probe–surface distance) is even more local [16]. Therefore, the local capacitance of the sample (understood here as the capacitance measured when the probe is located at a given point) can closely characterize the surface region closest to the probe.

The knowledge of the surface electric-potential distribution is important for studying different objects—from semiconductors to biological samples. It is the potential value that is the bridge that allows one to relate various observable properties to the local composition and structure of the samples. The widespread method of measuring a local potential with the aid of an electron beam has a rather low spatial resolution ( $\sim 100$  nm) and a poor voltage resolution (hundreds of millivolts) [17]; moreover, the method is destructive. A nanometer resolution is attained by using potentiometry based on scanning tunneling microscopy [18, 19]. However, it is required that the tunneling current flow through the sample, which limits the objects that can be studied by this method only to conducting samples. The AFM modification that allows one to measure electrostatic potentials removes the limits associated with the sample resistance and allows one to study nonconducting samples, which is very important, in particular, for microcircuits with dielectric layers and conducting elements whose surfaces are often strongly oxidized.

In the AFM modifications oriented to studies of electric properties, scanning is usually performed in the noncontact mode (although there is also a dynamic contact modification of the method) with the use of conducting cantilevers and probe tips and a low voltage applied between the tip and the sample. This voltage can be applied to the sample if the tip is grounded or, vice versa, to the tip if the sample is grounded. These two configurations require the use of different schemes of the tip–bimorph separation but yield equivalent results [20]. In the vicinity of the sample surface, the tip is subjected to the action of various forces—electrostatic, van der Waals, and capillary forces (if the surface is coated with a mobile adsorption layer) and also to the counteracting elasticity force from the cantilever.

We do not consider here the particular situations of capillary forces associated with the presence of a liquid (the interactions in the presence of a liquid on a neutral surface are discussed in [21] and those on a charged surface in [22]). Van der Waals forces and electrostatic interactions are observed in all the cases. It is possible to state that a “visiting card” of any force should indicate not only its absolute value but also the dependence of this value on the distance between the objects. In the theoretical analysis of electrostatic interactions, the tip–surface system was first modeled by a sphere of radius  $R$  spaced by a distance  $d$  from a planar conducting surface (or even by a conventional plane-parallel capacitor) [8, 9, 11, 23]. The first model predicts that the attraction force will be proportional to  $R/d$  for distances  $d \ll R$  and proportional to  $(R/d)^2$  for larger distances. Taking into account the elongated shape of the tip represented as a cone of a length  $L$  with the rounded “apex” of a radius  $R$  (Fig. 1), we arrive at a weaker law of force decrease: at  $L \gg d \gg R$ , this decrease is proportional to  $\ln(L/4d)$ , which reflects the contribution of the macroscopic part of the tip to the tip–surface interaction [24]. At small distances  $d \leq R$ , the main interaction is that between the tip apex and the surface, and we arrive again at a dependence inversely proportional with respect to  $d$  [24, 25]. It should be emphasized that a similar theoretical consideration was first made for the tip interaction with the conducting surface of the sample [24, 26–28], and, only recently, the influence of the geometric parameters of the tip on the forces acting between the tip and the dielectric sample taken into account [25, 29]. Numerical computations by the generalized image-charge method and the analytical expressions obtained for the limiting cases allowed one to establish the differences. For conducting samples, the main part is played by the absolute value of the apex radius, whereas, for dielectric samples, the force is affected by the tip shape and the height of the tip apex above the surface but not by the tip size (in the limit,  $d \rightarrow 0$ ).

The allowance made for the electrostatic cantilever–sample interaction under the conditions of an AFM experiment shows that the contribution to the force is practically independent of the distance  $d$  [27, 30]. However, as the computations for the system “macroscopic cantilever–mesoscopic tip (truncated cone)–tip apex (of the nanometer dimension)” [30] show, it is this interaction that dominates at  $d \geq 5$  nm. Therefore, the efficient sample area participating in the interaction considerably increases. To reduce the influence of the cantilever, one must thoroughly select the geometric parameters and use a nonconducting cantilever with a deposited narrow contact strip. It is much easier to suppress the cantilever contribution by measuring not the force but its gradients, because the latter are determined practically by the interaction with the tip apex alone [30].

The tip geometry also influences the van der Waals force, but to a lesser degree, so that under the conditions

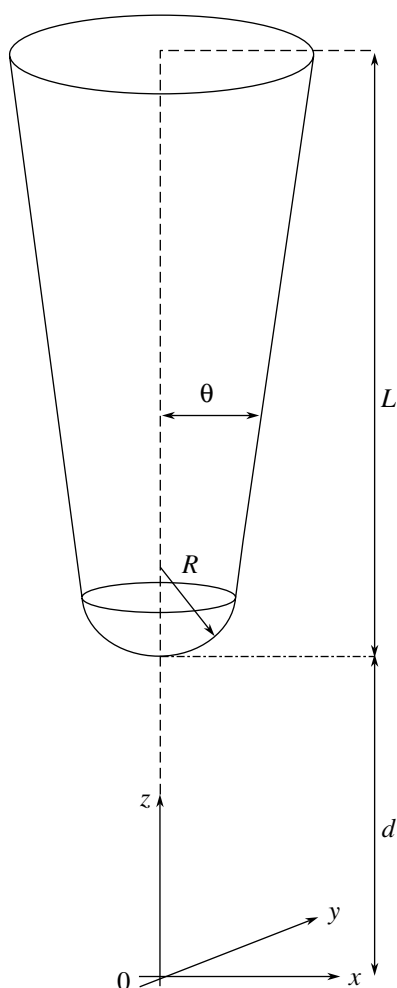


**Fig. 1.** Model of a cantilever tip and its geometric characteristics  $R$ ,  $L$ , and  $\theta$  used in calculations.

of the AFM experiment, the corrections are negligible [24]. At distances of an order of nanometers conventional for measurements of electric characteristics, the electrostatic attraction force exceeds the van der Waals force [8, 24]. This is clearly seen from measurements on graphite samples under various applied voltages, including the zero voltage [24]. Moreover, selective recording is also facilitated by the use of modulation methods. Nevertheless, because of the parallel topographic and electric measurements, the separation of the contributions due to these forces is still rather important [31–34]. Experimental data [24] also show that the interaction decreases with the distance from the surface rather slowly, in other words, the contribution of the macroscopic effects becomes rather important. A very important parameter in this case is tip-apex radius. The value of  $R$  directly affects the spatial resolution when studying electrostatic forces: as is shown in [35], at  $d \ll R$ , the spatial resolution is proportional to  $\sqrt{dR}$ . The methodological errors associated with the tip shape will be discussed somewhat later. Here, we consider the principle underlying the method.

## 2. THE PRINCIPLE UNDERLYING MEASUREMENTS OF ELECTRIC PARAMETERS

Electrostatic force can directly be determined after singling out its contribution to the cantilever deflection measured by an interferometer and with the use of the experimental dependence of the cantilever deflection on the tip height above the surface [36]. However, it is more efficient to determine the force gradient from a decrease in the amplitude of cantilever oscillations in the tapping mode with its approach to the surface, which is related to the resonance-frequency shift under the action of electrostatic forces [8].<sup>1</sup> It is this method that allows one to attain the atomic resolution [38, 39]. Another variant of force determination proceeds from the amplitude of cantilever oscillations under the applied periodic voltage between the cantilever and the sample [8]. If the applied-voltage frequency coincides with the resonance frequency of free oscillations of the cantilever, the amplitude is proportional to the electrostatic-force spectral component at the given frequency [40]. The formulas relating the amplitude of cantilever oscillations to the electrostatic force (or its gradient) and the system parameters for various types of probe and sample motion with respect to one another can be found in Chapter 11 [40]. In terms of capacitance, the most important of these parameters, the probe–sample system, is modeled by a flat capacitor or a sphere above the plane. The formulas are derived for the voltage applied between a conducting sample and a cantilever whose components are a constant bias and a harmonic component. A possible surface charge (if a sample is coated with a dielectric film) is also taken into account. The oscillations are considered not only at the resonance frequency but also at the frequency corresponding to the maximum steepness of the resonance curve. In principle, this allows one to determine the surface potential (the corresponding formula in [40] is given only in relative units), but the corresponding procedure is far from simple. It is not accidental that, although this possibility was considered in [8], no quantitative interpretation of the images in the potential units was made. Happily, as will be seen later, there exists a method for direct measuring the potential.

The general expression for the electrostatic force of interaction between the tip and the sample can be derived using the method of virtual work. One has to consider the work done by the given force at infinitesimal displacement  $\delta z$  of the tip along the  $z$  axis normal to the sample surface and, then, to differentiate the expression thus obtained with respect to this coordinate. If both sample and probe are connected to an external voltage source, the derivation should be performed at a constant potential. Then, the force  $F$  acting between the conducting probe and the sample is:

$$F = -1/2V^2\partial C/\partial z, \quad (1)$$

<sup>1</sup> The detailed consideration of dynamic noncontact AFM modes is made elsewhere [37].

where  $C$  is the capacitance of the probe–sample system and  $V$  is the potential difference between the probe and the sample, the contribution to which comes not only from the applied voltage  $V_{\text{app}}$  but also from the contact potential difference  $V_{\text{CPD}}$ ,  $V = V_{\text{app}} + V_{\text{CPD}}$ .

It should be remembered that the latter difference arises when two solids with different work functions are brought into electrical contact. In turn, the work function is the work spent on the transfer of an electron from the Fermi level of a solid into a vacuum. In the case of a contact, some electrons pass from the body with the lower work function  $\Phi_s$  into the body with the higher work function  $\Phi_m$ . Then, the first body acquires a positive charge, whereas the second acquires a negative one, and a field hindering further transitions arises. The thermodynamic equilibrium is attained when the electrochemical potentials of both bodies become equal, i.e., when  $eV_{\text{CPD}}^{\text{sm}} = \Phi_m - \Phi_s$ . The attraction force between such bodies also exists without external voltage because of different potential energies at a vacuum level at both surfaces,  $F = -\partial\Phi_{\text{vac}}/\partial z$ . In other words, within an accuracy of the coefficient equal to the electron charge and with due correction for the origin, the work function is the measure of the surface potential sought.

The work function, being determined, to a large degree, by a double electric layer at the solid boundary, is very sensitive to the state of the surface. It depends not only on the material but also on the crystallographic orientation of the surface and is considerably changed in the presence of either an oxide layer or adsorbed atoms. The work function is sensitive even to the states of adsorbed atoms. Therefore, the work function varies from one portion of a clean polycrystal surface to another (the regions possessing constant work functions are called patches), so that, in the vicinity of the surface, a certain field of patches is formed. Thus, the real situation is rather complicated. However, one also encounters considerable difficulties when modeling even rather simple situations.

Band diagrams in Fig. 2 illustrate the formation of the contact potential difference between metal and semiconductor samples with the front surfaces located at different distances, whereas their back surfaces are electrically connected. It is clearly seen that the situations for these materials are quite different: because of a high metal conductivity, the whole charge may be considered concentrated at the surface. In semiconductors having considerably lower carrier concentrations, the charged region extends into the bulk. With a decrease in the distance between the front surfaces, the thickness of the charged layer increases, and an ever-increasing fraction of  $V_{\text{CPD}}$  would correspond to the region of the bulk charge, and an ever-decreasing fraction, to the vacuum gap (Fig. 2). The same is true for the distribution of the external voltage applied between the tip and the sample—at the given  $V_{\text{app}}$  value, the poten-

tial of the semiconductor surface depends on the sample–tip distance. Therefore, strictly speaking, Eq. (1) describing the force is valid only for conducting probes and samples. If a probe or a sample is a semiconductor (in studies of semiconductor materials or the use of silicon cantilevers), one must take into account the fact that the probe–sample capacitance stops being passive and starts depending on voltage. The problem becomes even more complicated if one takes into account the surface states, which can considerably influence band bending at the surface of a semiconductor.

This fact has not passed unnoticed. Electrostatic interactions with the participation of semiconductor objects were analyzed theoretically with the invocation of method of images. The corresponding electrostatic problems were considered for a point charge above a semiconductor surface [41] and also for the simplest model of two flat metal and semiconductor plates [42]. If the distance between the objects is on the order of the thickness of the bulk-charge layer, some specific features are observed. The force depends on the distance differently than in the case of two interacting conductors. It was established [42] that this effect manifests itself differently for different states of the subsurface region (in this region, depending on the voltage applied, either the enrichment, depletion, or inversion mode can be observed). At distances less than several depleted-layer thicknesses, the force depends on distance and voltage differently than in the case of two metal objects. The deviation from a quadratic increase in force with an applied voltage (characteristic of interaction of conductors) was also observed in [43]. The interaction force was calculated for the system “metal probe– $n$ -type semiconductor (Si) coated with an oxide layer of the given thickness” also in the plane-parallel geometry. At the positive polarity of the applied constant voltage corresponding to an increase in the majority-carrier concentration close to the surface, the force remains proportional to  $V_{\text{app}}^2$ . At a considerable negative bias, the inflow of minority carriers results in the inversion of the conductivity type in the subsurface region and the  $F(V_{\text{app}})$  dependence asymptotically tends to a parabola. However, at low negative values,  $V_{\text{app}} \sim (-1)–(-2)$ , in the depletion mode, the force increases with an increase in bias more slowly because of the effect of the positive charge of impurity atoms that remained uncompensated after the pushing-away of majority carriers from the subsurface region. This tendency is the more pronounced the closer the probe to the surface and the lower the donor concentration. Therefore, for moderately doped semiconductors, the influence of the space charge should be taken into account. However, as shown in [42, 44], heavily doped Si cantilevers can be regarded as metal ones.

Nevertheless, in practical studies, the above effects have not been not taken into account as yet, and the calculations are still based on Eq. (1), even for semiconductor samples [45]. Only when studying dielectrics

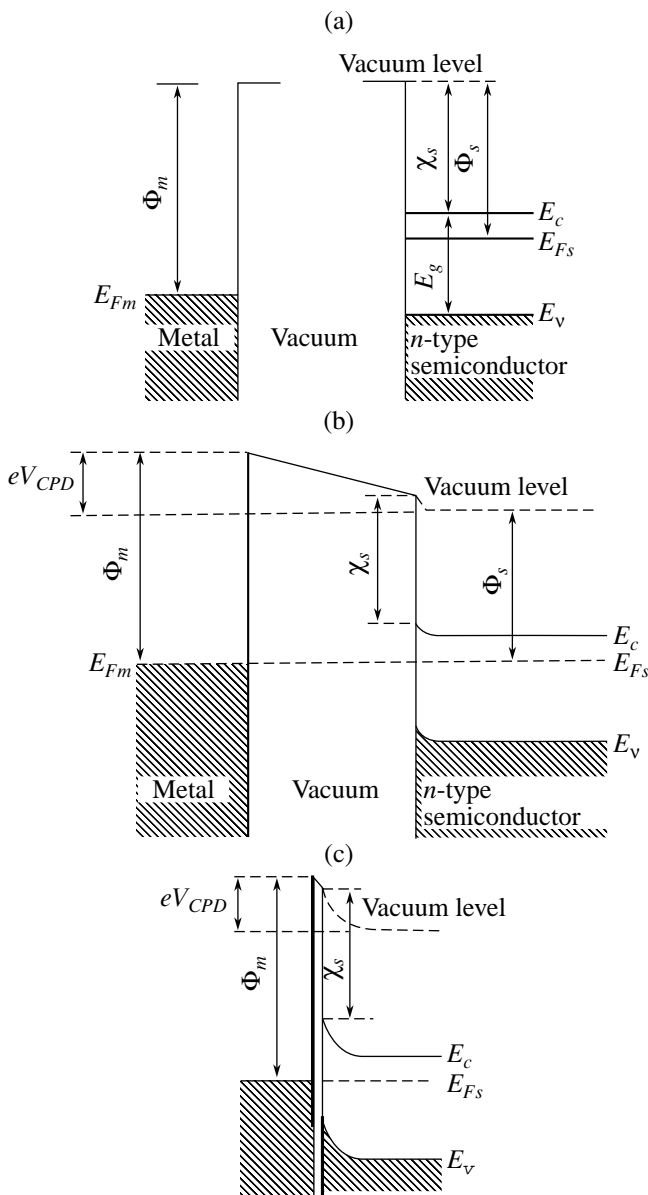


**Fig. 2.** Illustrating the formation of a contact potential difference  $V_{CPD}$  in the system metal- $n$ -type semiconductor (the work function of the metal is higher than that of the semiconductor,  $\Phi_m > \Phi_s$ ). Notation of band diagrams:  $E_{Fm}$  is the Fermi level in the metal,  $E_{Fs}$  is the Fermi level in the semiconductor,  $E_c$  is the conduction-band bottom,  $E_v$  is the valence-band top,  $E_g$  is the band gap, and  $\chi_s$  is the electron affinity of the semiconductor. (a) No contact between the metal and semiconductor, (b) electric contact between the metal and semiconductor spaced by a considerable distance, and (c) the objects are almost in contact with one another.

does one usually take into account an additional electrical field induced by surface charges and introduce into the force the corresponding contribution expressed in terms of  $\sigma$  (surface charge density) [12, 33, 36, 45, 46]. An alternative approach is the use of the Born approximation of the perturbation theory for the allowance for the force in the case where the field is distorted by a sur-

face charge [47]. In fact, in this case  $\sigma$  itself becomes the main object of the study. However, we return back to initial Eq. (1).

Modulating the applied voltage  $V_{app} = V_{DC} + V_{AC} \sin \omega t$ , one can represent force (1) as a sum of three components:

the constant force,

$$F_{DC} = -1/2 \partial C / \partial z \{ (V_{CPD} + V_{DC})^2 + 1/2 V_{AC}^2 \}, \quad (2)$$

the force varying with the fundamental frequency  $\omega$  (the first harmonic),

$$F_{\omega} = -\partial C / \partial z (V_{CPD} + V_{DC}) V_{AC} \sin \omega t = F_1 \sin \omega t, \quad (3)$$

and one more harmonic force varying with a double frequency (the second harmonic),

$$F_{2\omega} = 1/4 \partial C / \partial z V_{AC}^2 \cos 2\omega t = F_2 \cos 2\omega t. \quad (4)$$

It is seen that the last component depends only on the probe-sample capacitance  $\partial C / \partial z$ , whereas the force  $F_{\omega}$  also contains the information on the contact potential difference. These quantities can be determined by measuring the oscillation characteristics of the cantilever under the action of these periodic forces. If the cantilever moves in the oscillation mode for the topographic measurements, then the third spectral component is observed at the frequency  $\omega_r$ . In principle, the heterodyne interferometer allows one to record the cantilever deflections at several frequencies simultaneously [20] if the frequencies of the corresponding signals are sufficiently separated, as in Fig. 3. Figure 3 shows the frequency spectrum of cantilever oscillations [48]: similar to the tapping mode in AFM, the signal at the free-motion resonance frequency  $\omega$  is used to perform the topography measurements, whereas the frequency  $\omega$  of the modulating electric signal is selected in such a way that both this frequency and the second harmonic are outside the resonance frequency band. Strictly speaking, because of the nonlinear nature of the cantilever-surface interaction, the free oscillations of the cantilever are anharmonic [49, 50], whereas the contribution of higher harmonics is negligible [51] and, in this case, can be ignored. The block-diagram of a modern multifunctional-type setup [48], which enables one to use the possibilities of the so-called electrostatic force microscopy, is shown in Fig. 4. However, researchers often use more specialized apparatus for measuring a potential or a capacitance. In the first case, it is scanning Kelvin probe microscopy; in the second scanning capacitance microscopy. After making some preliminary remarks, we consider the characteristics of both methods.

Since the methods discussed are rather new, both the terminology and the technical characteristics of the setups used are somewhat inconsistent. Thus, the parameters of the oscillating probe systems can considerably differ. As a rule, the cantilevers used are rather rigid and have the spring constant  $k$  ranging from several new-

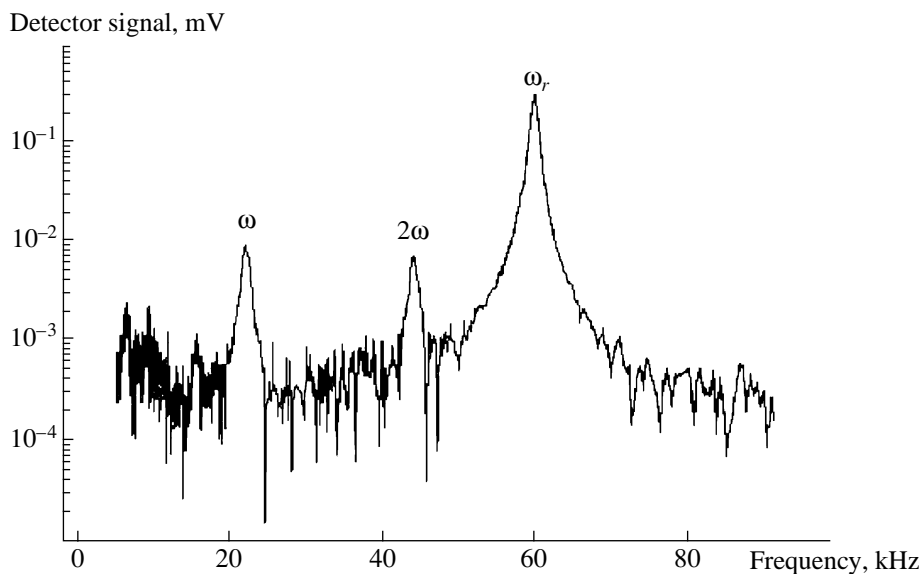


**Fig. 3.** Cantilever frequency spectrum with a resonance frequency of 60 kHz measured with the aid of a lock-in amplifier at a constant bias voltage of 0.5 V and a.c. frequency of 21 kHz (in the absence of feedback compensating the contact potential difference) [48].

tons to several tens of newtons per meter (most often, 20–30 N/m) and are prepared from heavily doped silicon or, sometimes, also from  $\text{Si}_3\text{N}_4$  (with a conducting coating) or tungsten. For attaining a higher conductivity, silicon cantilevers may be coated with Au, Co, Cr, or PtIr layers. Unfortunately, these layers are rapidly worn out in air [52]; pure silicon is rapidly oxidized. Comparing the stability of potential images obtained with the aid of silicon cantilevers coated and not coated with a metal favors uncoated cantilevers [53]. It seems that it is better to increase the cantilever conductivity by depositing onto it (chemical vapor deposition) boron-doped thin diamond films. Such coatings may also be used for measuring currents in the contact mode [54]. Similar cantilevers were also used in studies by scanning Kelvin microscopy [55]. The apex radius  $R$  usually lies within 5–40 nm, whereas the conventional oscillation amplitude lies within 10–20 nm. The requirements for tips set by the problems of “electric” AFM and the comparative analysis of the tip quality, including the quality of diamond tips, can be found in [56]. The  $Q$  values of cantilevers as oscillating systems do not exceed 100–200 in air, but, in vacuum, they increase up to 1000–2000 [57] and even higher (in [31], the  $Q$  factor attains a value of 38 000). A better design could have increased the  $Q$  values further, but it is not justified because of narrowing of the bandwidth of the system and an increase in the response time [58]. The free-motion resonance frequencies  $f_0$  of the cantilevers range from tens to hundreds of kilohertz. Proceeding from various considerations, the frequency  $\omega$  of the modulating voltage can be chosen to be the first and the second resonance frequencies or a lower frequency (2–3 kHz or even 300 Hz). The amplitude of a.c. voltage

$V_{AC}$  usually varies from tenths of a volt up to several volts.

Thus, the optimum parameters of the system have not been established as yet, so that all the experimenters continue indicating the technical data of their experiments. As to the spatial resolution, some authors indicate the atomic resolution for GaAs(110) [31], Ag/Si(111) [38, 59], Au/Si(111) [39], and Sb/Si(111) [60].

### 3. SCANNING KELVIN PROBE MICROSCOPY

Scanning Kelvin Probe Force Microscopy, abbreviated in the literature as KPM, SKPM, KPFM, KFM, and SKFM, inherited its name from the method of measuring a contact potential difference suggested by Lord Kelvin as far back as 1898. In this method (also called the method of dynamic capacitor), two samples form a flat capacitor. The electrically connected plates oscillate relative to one another, and the potential difference between the plates is measured. If the plates are not charged, the voltage equals zero and remains zero during plate oscillations. But if the plates have different work functions, a charge arises and the capacitance varying with the distance gives rise to the corresponding change in the voltage. In series switching into the circuit of a d.c. source, one may select its voltage  $V_{app}$  in such a way that it is equal to  $V_{CPD}$  but has the opposite sign. Then, the charges at the plates become fully compensated, and the oscillations of the voltage measured at the vibrating plates cease, which indicates that, now,  $V_{app} = V_{CPD}$ . Thus, determining  $V_{CPD}$  in such a way and knowing the work function of one of the plates (test plate), one can determine the work function of the sec-



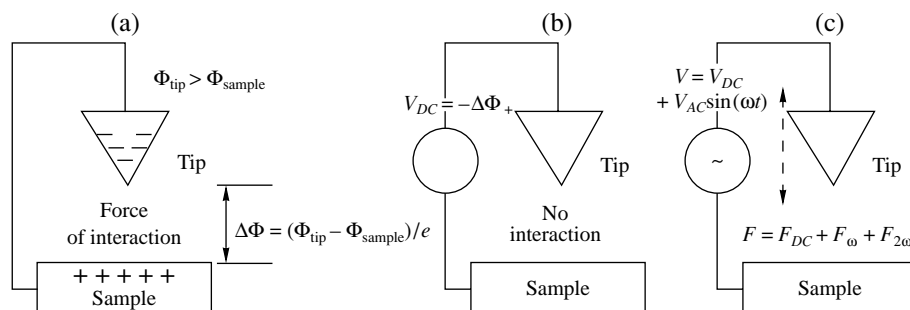


**Fig. 5.** Illustrating the compensation principle in Kelvin microscopy [65]. (a) Because of a contact potential difference between the tip and the sample, the electrostatic interaction takes place without application of any voltage (for definiteness, it is assumed that the tip work function  $\Phi_{\text{tip}}$  exceeds the sample work function  $\Phi_{\text{sample}}$ ); (b) an appropriately chosen applied constant voltage decreases the interaction force to zero; (c) the application of an alternating voltage gives rise to tip oscillations.

onance and the voltage is modulated at the frequency of the first or second resonance or at a considerably lower frequency. During the first pass along the given scan line, the profile is recorded in the tapping mode (the cantilever oscillations are excited close to the surface by a bimorph). In this case, the feedback in the control system of vertical motion maintains a constant amplitude of cantilever oscillations (amplitude modulation) or a constant shift of its resonance frequency (frequency modulation). Thus, one determines points equidistant from the surface (the force gradients at these points are the same) [58]. Then, the feedback is switched off, the mechanical excitation of oscillations is ceased, and the cantilever rises from the sample to a distance from several to several tens of nanometers (the so-called lift-mode) and second scanning is performed at a constant distance (the tip goes along the trajectory, repeating the profile recorded earlier) but under an applied voltage  $V_{DC} + V_{AC}\sin\omega t$ . The new feedback establishes the bias  $V_{DC}$  in such a way that there is no signal at the frequency  $\omega$ . The details of the optimum feedback tuning can be found in [53]. The corresponding  $V_{DC}$  values after the sign reversal are the  $V_{CPD}$  values at each point of the line (it should be indicated that, in a number of studies, another sign convention is used).

The minimum potential thus measured depends on the level at which the alternating-voltage-induced oscillations can be separated. It seems that the thermal and optical noise should contribute to the error of the measured amplitude of cantilever oscillations. In this case, the optical noise is negligible [23], and, therefore, the minimum potential is recorded when the amplitude of induced cantilever oscillations attains a value on the order of random thermal fluctuations [67]

$$V_{\min} = \sqrt{(2k_B T k_B / \pi^3 Q f_0) d / (\epsilon_0 V_{AC} R)}, \quad (5)$$

where  $k_B$  is the Boltzmann constant,  $T$  is the temperature,  $\epsilon_0$  is the dielectric constant in vacuum, and  $B$  is the bandwidth. At the parameter values used in [68], the resolution attains a value of 0.1 mV, i.e., is at the level

of earlier studies [67]. However, it seems that it can be improved by two orders of magnitude by performing measurements in a sufficiently high vacuum at low temperatures.

In practice, not only the instrumental errors influence the potential, but also some additional factors associated with the physics of the phenomenon. It turns out that the recorded potential  $\Phi_{\text{meas}}$  depends on such factors as the tip used, the height of the tip location above the surface, and the amplitude of the applied alternating voltage, and the recorded changes may exceed the expected error. Then, the question arises why such a situation is possible, how reliable the results obtained are, and whether they may be compared with one another and with the data obtained by other independent methods.

The simplest factor is the effect of a tip, because one measures a contact potential difference that strongly depends on the tip state and the presence there of defects, oxide layers, contaminations, etc. Thus, in [69], after the change of the tip, the measured surface potential of a silicon sample changed by 30–50% (in some cases, even by 100%) (Fig. 6). Therefore, the reproducible results can be obtained only in high vacuum in order to avoid, at least, adsorption from air. Such ultra-high vacuum setups (with the residual pressure  $\leq 10^{-10}$  mbar) have already been constructed [59, 70], but, in fact, most studies are still performed in air or, at best, in an atmosphere of dehydrated gas. However, even high-vacuum experiments cannot guarantee tip homogeneity: it is most probable that the tip surface consists of patches—regions having different work functions (because of steps, nonuniform coating, etc.). Burnham *et al.* [71] believe that it is the patches on the tip and sample that are responsible for the long-range component of the interaction force acting between the tip and sample in the case of no applied voltage.

The fields of the sample patches always existing above the inhomogeneous (with respect to the work function) surface play an important role in method accuracy. The mechanism of contrast formation in SKPM and the method resolution were analyzed theo-

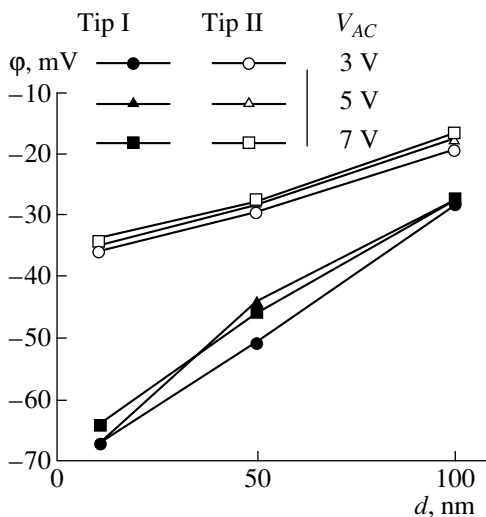


**Fig. 6.** Measured surface potential of  $\phi$  Si(100) surface for two different tips as a function of the scanning parameter (the height  $d$  of the tip location above the surface) at three different alternating-voltage amplitudes [69].

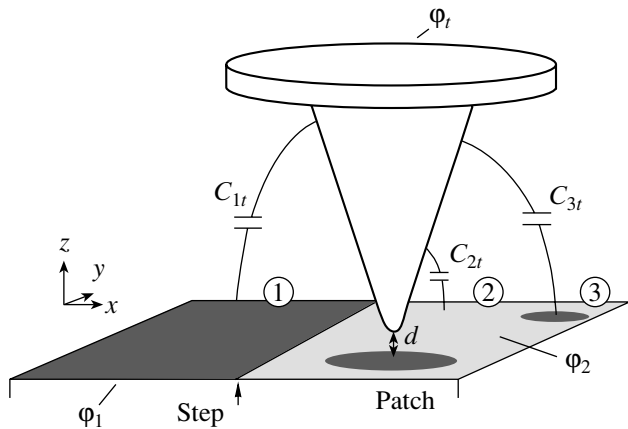


**Fig. 7.** Model of a surface consisting of ideal conductors with different potentials  $\phi_i$  [72], which interact with the tip via the mutual capacitance  $C_{ij}$  [72].

retically on a sample consisting of a set of  $n$  ideal conductors with different constant potentials  $\phi_i$  [72]. The energy of electrostatic interaction in the tip–surface system was calculated with due regard for the capacitance coupling between the tip and various patches (shown in Fig. 7 by capacitance  $C_{it}$ ) and the capacitance coupling between the patches themselves,  $C_{ij}$ ; then, the force acting on the tip was determined. Under the conditions of SKPM, the potential  $\phi_{DC}$  equals not the exact value of  $\phi_i$  for the patch located directly under the tip—it equals the weighted value averaged over the surface, where the role of the coefficients is played by the  $\partial C_{ii}/\partial z$  derivatives:

$$\phi_{DC} = \left( \sum_{i=1}^n \partial C_{ii} / \partial z \phi_i \right) / \left( \sum_{i=1}^n \partial C_{ii} / \partial z \right). \quad (6)$$

In the limit of infinitely small regions, Eq. (6) is transformed into a two-dimensional convolution of the real potential with a certain transfer function. Comparing the results of the numerical simulation of two typical situations—the potential distributions in the form of a patch and a step—with the experimental data obtained on specially prepared test structures showed good agreement between the calculated and experimental data. It is important for the method efficiency that both real and simulated measurements in the vicinity of the boundary characterized by a dramatic change of the potential give a smoothed pattern with a continuously varying  $\phi$  in the transient region. The calculations performed for different tip geometries showed that this smoothing is feebly marked for thin long tips with a blunt apex (high  $R$  values). It is this configuration that ensures the prevalence of the local electrostatic interaction over the nonlocal interaction, so that the information thus obtained relates mainly to the surface region lying directly under the tip.

Capacitance in Eq. (6) depends on the tip shape (of course, with a certain scatter for different tips) and the height of its location above the surface. Therefore, the variations in the measured potential  $\phi_{\text{meas}}$  caused by the tip change and its locations at different heights above the surface observed in the studies of inhomogeneous samples with the traces of wear in air [69] can be associated with the methodical limitations considered above. The influence of the tip height on the resolution was studied experimentally (on the  $p$ – $n$ -junction in GaP and the steps on GaAs and HOPG samples in high vacuum) and theoretically (a tip was modeled by a “staircase” of flat capacitors switched in parallel, with the semiconductor effect being ignored). The “diffusion” of the work function in the region of its dramatic change and its decrease observed during measurements become more pronounced with an increase of the height, which can be satisfactorily described within the framework of the approximate model considered above. (The possibility of working at smaller heights can also increase the resolution in high-vacuum setups [73].) It should be emphasized that, as earlier, the key role in the above calculations is played by surface inhomogeneity with respect to the work function.

However, the potential measured in high vacuum at heights less than 50 nm on a test atomically smooth HOPG sample also varied [44]. This effect was different for different cantilevers. Thus, for new cantilevers, the effect was on the order of several millivolts, but it dramatically increased up to hundreds of millivolts after the tip contact with the sample. It seems that, here, the key part is played by the tip state—with a decrease of the distance, the tip apex starts playing the most important role and its metal coating gradually wears out. In any case, the assumption that the measured potential depends on the distance because of the incomplete compensation of  $V_{CPD}$  [74] is not confirmed here. (Since the amplitude of the recorded signal can be

reduced to zero only within the experimental error, then, in virtue of Eq. (3), the  $\varphi_{\text{meas}}$  value depends on the quantity reciprocal to  $\partial C/\partial z$ .) In [74], the  $\partial C(z)/\partial z$  dependence was calculated theoretically by summing up the contributions that come to the capacitance from the individual parts of a tip of the given shape which lie at different distances from the surface. The plot of the reciprocal quantity repeats the shape of the  $\varphi_{\text{meas}}(z)$  curve. On the contrary, a  $\partial C(z)/\partial z$  dependence for HOPG samples at the same heights as  $\varphi_{\text{meas}}$  was recorded experimentally [44] in accordance with Eq. (4). It turned out that this curve cannot be used to explain the experimental changes in  $\varphi_{\text{meas}}$ . Sommerhalter *et al.* [44] believe that, using the appropriately selected feedback parameters, it is possible to reduce the deflection caused by the incomplete compensation of  $V_{CPD}$  to the noise level of the system. Nevertheless, Efimov and Cohen [55] suggested a special algorithm for improving the potential image by separating from it the component associated with “undercompensation” of  $V_{CPD}$  for tips having certain geometries. Gil *et al.* [30] explain the sensitivity of the SKPM method to the height of the tip location by the contribution of the interaction of all the parts of the cantilever–tip system. As a result, one measures, in fact, the weighted potential value (similar to Eq. (6)). However, as was indicated above, this interpretation of the  $\varphi_{\text{meas}}(d)$  dependence is valid only for inhomogeneous surfaces.

The effect of  $V_{AC}$  on the measured  $\varphi_{\text{meas}}$  value (less pronounced in Fig. 6 than the influence of the height variation or tip change) is of a pure semiconductor nature. Leng *et al.* [75] observed the changes in  $\varphi_{\text{meas}}$  up to 1 V in air with an increase in  $V_{AC}$  from 1 to 7 V for a disordered GaInP sample and indicated that no such dependence is observed for clean metal samples and tips. Neither was it observed for HOPG samples [44]. However, the dependence was quite pronounced for a *p*-WSe<sub>2</sub> sample [44]. As was to be expected, the dependence was more pronounced at smaller tip–surface distances because, at such distances, the electric field penetrates more deeply into a semiconductor and the band bending becomes more pronounced (Fig. 2). The  $\varphi_{\text{meas}}(V_{AC})$  dependence is caused by different charging of the surface in the sequence of half-periods of positive and negative polarities (in the depleted state, the potential varies much more pronouncedly than in the enriched state). It should be noted that the nonsymmetric tip–semiconductor surface interaction with the change of the voltage polarity was predicted theoretically as far back as 1992 [43] for all the three force components,  $F_{DC}$ ,  $F_{\omega}$ , and  $F_{2\omega}$ . The necessity of taking this into account was also indicated in [76].

Therefore, to reduce the influence of  $V_{AC}$  on the measured potential, one has to study semiconductor materials at the minimum  $V_{AC}$  values (on the order of 100 mV). However, it is seen from Eqs. (3) and (5) that, to increase the method sensitivity, one has to increase

the  $V_{AC}$  value at least by an order of magnitude, i.e., to increase it up to several volts (this would increase the amplitude of oscillations induced by the force  $F_{\omega}$ ). These requirements set to  $V_{AC}$  become contradictory for the scheme of amplitude modulation described above, in which the complete compensation of the contact potential difference  $V_{CPD}$  (attained by the application of the voltage  $V_{DC}$ ) can be seen from the zero oscillation amplitude at the frequency  $\omega$  (force measurement [57, 66, 70]). It is expedient to use the second resonance frequency of the cantilever as an alternating-voltage frequency [57]. This allows one to attain a resolution of 5 mV at the small amplitude  $V_{AC}$  [44]. The alternative is the use of the frequency-modulation method (force-gradient measurement): the signal circuit should also have a frequency demodulator to control the variation of the oscillation frequency caused by the electrostatic interaction (the frequency shift oscillates with the frequency of the alternating voltage [38, 59]). In this case, the bias equal to the contact potential difference is determined from the absence of frequency oscillations. However, it turned out that, to attain an energy resolution similar to that in the method of the amplitude modulation, one has to use higher  $V_{AC}$  values ( $\geq 2$  V) [44]. On the other hand, the spatial resolution at the frequency modulation is higher (as was indicated above, in terms of the force gradient, the main part in the interaction is played by the tip apex). In the determination of the force, which is less dependent on the distance than its gradient, an important role is played by the averaging effect of the tip and cantilever. The latter effect increases the region around the probe that participates in the interaction. At the same time, at the amplitude modulation, the dependence of the potential measured for inhomogeneous surface on the tip height above the surface is weaker [77]. The influence of the tip geometry on the spatial resolution of SKPM has been studied experimentally [77] and it was shown that, in accordance with the prediction made in [72], the highest resolution is observed for long tips.

The accuracy of the determination of the surface potential can be increased by invoking some additional information on the signal phase [78]. Analysis shows that, unless the absolute  $V_{DC}$  value is lower than the contact potential difference, the phase of the component of the electrostatic force at the frequency  $\omega$  is shifted by  $\pm 180^\circ$  with respect to the applied alternating signal. If  $|V_{DC}|$  exceeds  $|V_{CPD}|$ , this phase difference goes to zero, i.e., at  $V_{DC} = -V_{CPD}$ , the signal phase dramatically changes, which can readily be detected experimentally. In turn, this allows one to fix the moment of the complete compensation of the contact potential difference.

New possibilities for studying semiconductors are provided by the use of near-field optical waveguides with metal coatings as cantilevers. This allows one to illuminate the sample locally and, thus, to complement the Kelvin microscopy with photovoltage measure-

ments (surface photovoltage method, SPV) [79]. Photon absorption gives rise to the formation of electron-hole pairs that are separated in the field of the volume charge in the vicinity of the surface (appearance of photovoltage). In the subsurface region, the carrier concentration increases and band bending (surface potential) is changed. If the incident light is sufficiently intense, flat bands may arise (the photovoltage attains the saturation that allows one to determine the potential barrier height). Varying the wavelength of the monochromatic radiation, it is possible to initiate transitions of electrons from various initial states (from the valence band or the levels in the forbidden band). Then, the change in the work function allows one to obtain information on the distribution of the surface states, recombination centers, etc. Experiments show [79] that new cantilevers ensure potential measurements with an accuracy not less than the accuracy attained by the traditional methods and allow one to record the changes of the potential under illumination. An interesting technical solution for SKPM is suggested in [80]—to use the carbon nanotubes as probes, which should increase the spatial resolution of the method.

Finally, let us answer the question whether it is possible to use SKPM for extracting the absolute quantitative information on the work function. Brushan and Goldade [69], who work in an air atmosphere, have a rather pessimistic opinion. They believe that one can obtain only the qualitative information about the potential variation along the surface. The measurements performed in the  $N_2$  atmosphere [78] are quite consistent with the known data. It is recommended to anneal both samples and tips prior to measurements in order to remove the adsorbed layers, in particular, water [81]. It was shown [70] that, under the conditions of high vacuum, the absolute measurements are rather reliable if each concrete cantilever is preliminarily calibrated against the test surface with the known work function.

The number of problems solved by SKPM is rather large. For crystals, the method allows one to reveal and characterize even feebly marked inhomogeneities. The first SKPM studies allowed one to visualize Pd micro-particles on a gold substrate, grains of polycrystalline gold, and their grain boundaries, and observe the changes in the dipole layer at the steps of an as-cleaved HOPG sample [67, 82]. Considering the cross section of a GaInP film on the GaAs substrate, Leng *et al.* [75] managed to distinguish atomically ordered and disordered (with respect to alternation of Ga and In atoms in the (111) planes) submicron regions. Kitamura and Iwatsuki [59], performing experiments under high vacuum, attained the atomic resolution and identified the phases with the  $5 \times 2$  and  $7 \times 7$  surface structures in the Au/Si(111) system (the work function for the former regions was higher by 0.5 eV than for the latter ones) with dimensions of tens of nanometers. Sputtering Ag onto the *n*-Si(111)  $7 \times 7$  surface, Kitamura *et al.* [38] and Kitamura and Iwasaki [59] managed to separate polycrystalline Ag clusters and hexagonal Ag(111)

islands (the difference in their work functions attained 20 meV; the contrast against the silicon background attained 10 meV). Kitamura *et al.* [39] studied in detail the Au clusters on the *n*- and *p*-types Si(111)  $7 \times 7$  surfaces and revealed no differences in the image contrast. Therefore, they suggested that, at an atomic resolution, the contrast is determined mainly by the surface electron density, whereas the calculation of the “true” work function requires the use of the average potential difference between the cluster and substrate. However, Kitamura *et al.* [39] consider the notion of the true work function in association with the position of the Fermi level in the crystal bulk, whereas, on the surface of a semiconductor, the bands are often bent because of the surface states. Close values of the surface potential for the *p*- and *n*-type GaAlSbAs samples were also observed in [83] and were explained by the presence of charged traps on the surface. The shift of the Fermi level with respect to the bulk (different for different sample thicknesses) was clearly observed on InAs(110) by the SKPM method [81]. A jump of the Fermi level in the vicinity of steps on as-cleaved *n*- and *p*-type GaAs(110) surfaces observed in [70] was attributed to the action of the localized states of atoms with a distorted coordination. The work function of the monolayer of  $TiO_2$  islands of nanometer sizes also increases with respect to the work function of the remaining atomically smooth  $TiO_2(110)$  surface, but, in this case, continuously—it attains the maximum in the island centers [84]. This was explained by the dipole-type polarization in the vicinity of the island boundaries. Sommerhalter *et al.* [70] indicate that SKPM may also be used to detect impurity centers and determine the sign of their charges (they considered the *p*-type  $WSe_2(0001)$  surface cleaved in vacuum). Measurements at an atomic resolution allowed one to identify single species, i.e., to separate the Si and Sb atoms (the surface potential of the latter atoms was higher by 0.2 eV) on the Si(111)  $5\sqrt{3} \times 5\sqrt{3}$ -Sb (it should be remembered that the topographic image at an atomic resolution fails to distinguish between these atoms) [60]. However, the above value is not consistent with the difference between the work functions of bulk samples or with the difference in the ionization energy of the isolated atoms. Thus, the interpretation of the results obtained requires the detailed theoretical analysis of the energy band of the atoms adsorbed on concrete surfaces. Without such an analysis, it is impossible to reliably establish the mechanism of formation of potential images on the atomic scale [39, 60].

SKPM also turned out to be very a convenient method for studying the wear of materials due to friction [69], analysis of galvanic effects in corrosion of aluminum-based alloys [85], and detection of intermetallic inclusions in alloys ( $Al_2Cu$  in the Al–Cu system) [68]. The transition from the qualitative to quantitative interpretation of the experimental data opened new vistas for control for electric processes in various devices

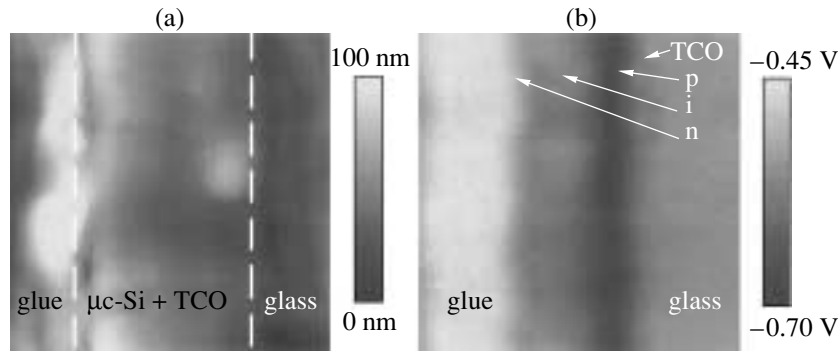


**Fig. 8.** Topographic image (left) and the corresponding surface potential scan (right) of cross-sectioned *pin*-diode prepared from microcrystalline silicon. Scan size is  $3.5 \times 3.5 \mu\text{m}$  [88].

in microelectronics—from thin-film InGaAs resistors [74] and *p-n* junctions on Si [57, 86] to complex heterostructures [86–88].<sup>2</sup> Thus, it is possible to record a built-in potential. Its comparison with the calculated profile revealed the incomplete donor ionization in laser-based *n<sup>+</sup>*-InP/InGaAsP/*p<sup>+</sup>*-InP diodes [87] and explained insufficiently efficient collection of carriers associated with defect and impurity distributions in solar elements based on microcrystalline silicon (Fig. 8) [88]. Studying the potential distribution in the cross section of a multilayer  $\text{Al}_{0.3}\text{Ga}_{0.7}\text{As}/\text{GaAs}$  structure, Tanimoto and Vatel [86] proved, using secondary-ion mass spectroscopy (SIMS), that the SKPM method is sensitive to the Al content in each layer. The measurements performed on illuminated samples allowed one to determine the change in the depleted-layer width, to study the transition to flat bands, and to draw conclusions on the band structure of the cleavage. Applying the bias voltage to laser GaAlSbAs/GaSb(100) diodes cleaved along the (110) surface, one can directly determine the voltage drop at the heterojunction and the active region of the device [83]. It was revealed that, in junction-based GaP diodes, the potential distribution (whose change turned out to be much more pronounced than the applied bias) depends on the electron transitions from shallow localized levels to the conduction band occurring under the action of emitted light [89]. Koley and Spencer [90] recorded the potential distribution around a single dislocation in *n*-GaAs films and  $\text{Al}_{0.35}\text{Ga}_{0.65}\text{N}/\text{GaN}$  heterostructures (Fig. 9), determined the position of the Fermi level in both film and heterostructure, and suggested a band diagram with acceptor dislocation levels.

#### 4. ELECTROSTATIC FORCE MICROSCOPY

As was indicated above, electrostatic force microscopy (EFM) is a combined method that allows one to

<sup>2</sup> In this case, when using Eq. (1), one has to take into account in the expression for voltage  $V$  also the voltage  $V_{\text{ind}}$  induced on the surface and associated with the device operation. In other words, the image contrast is determined by the sum  $V_{\text{CPD}} + V_{\text{ind}}$ .

measure the electrostatic force—usually both its harmonics,  $F_{\omega}$  and  $F_{2\omega}$ . In 1988, when Martin *et al.* [8] first measured the electrostatic force using an atomic force microscope in the range of distances from several to 170 nm and determined the minimum recordable force  $10^{-10}$  N by this method, the term *EFM* had not been coined. Schönwenberger and Alvarado [11] recorded a value of  $14 \times 10^{-9}$  N. Today, when we have instruments that can operate in vacuum and also at low (including helium) temperatures, it is also possible to measure forces less than  $10^{-12}$  N [91]. Among the pioneers of the method are, also, Stern [10] and Terris [12], with co-authors, who tried to use electrostatic forces to visualize the charge distributions on the surfaces of dielectric samples. First, they manage to record the appearance of such a charge by analyzing the contours of constant force gradient measured in the conventional tapping mode of AFM. Because of the Coulomb attraction between the charge on the surface and the corresponding charge induced at the tip, the contour shows sharp peaks. It is possible to single out the charge peaks against the background of topographic images and determine the charge sign by applying a constant bias  $V_{\text{DC}}$  of different signs and values to the metal electrode under the film [10, 92]. The application of the bias would change the charge induced at the tip and, thus, also the force of interaction, which, in turn, could change the image contrast up to its reversal (Fig. 10). However, the necessity of multiple scanning at various  $V_{\text{DC}}$  values led the authors to the idea of modifying the method. Working, as usual, in the tapping mode, they applied a.c. voltage  $V_{\text{AC}}\sin\omega t$  between the cantilever and the metal electrode under the dielectric sample with a frequency much lower than the oscillation frequency in the vicinity of the resonance. Then, the existence of the surface charge can be established from the presence or absence of an additional modulation of the force gradient at the frequency  $\omega$  [12, 92]. The component with the frequency  $\omega$  is responsible for the charge imaging, with the charge sign being determined by the signal phase. Thus, Terris *et al.* [92] recorded simultaneously within one scan the signals at different frequencies (as

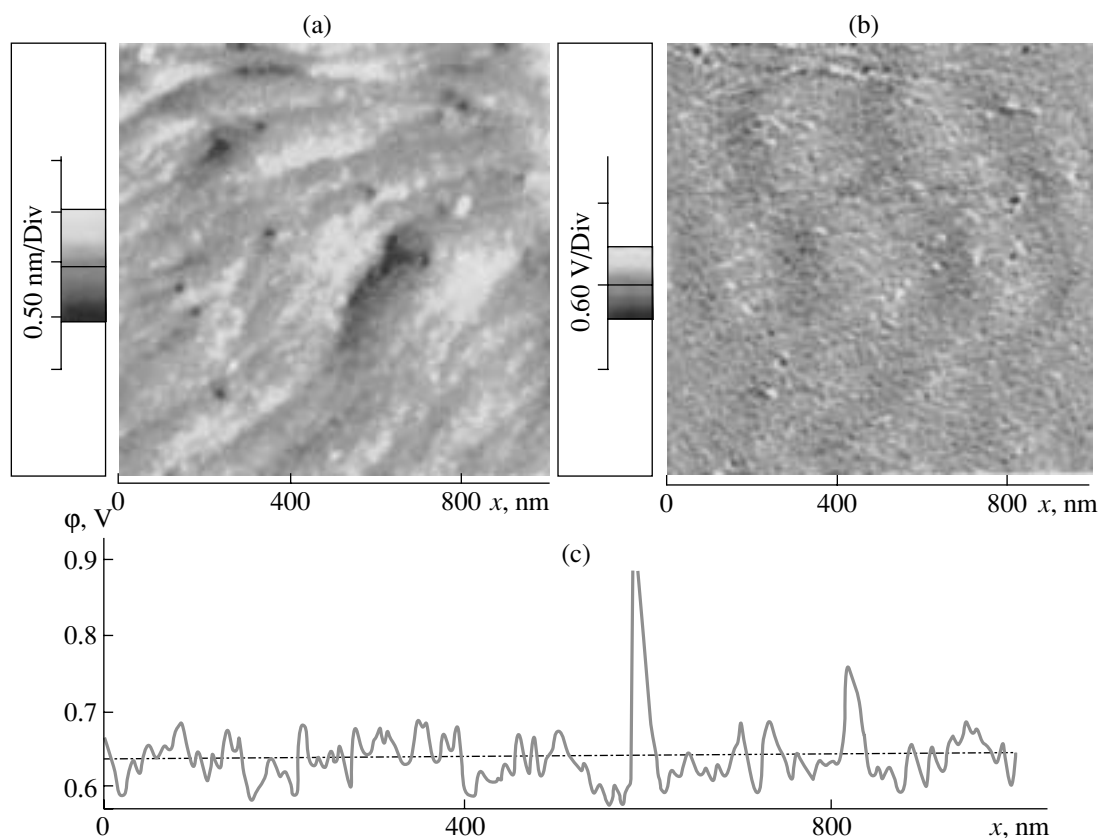


**Fig. 9.** (a) Topography of an *n*-GaN surface, (b) surface potential image ( $1 \times 1 \mu\text{m}$ ) taken simultaneously on unintentionally doped *n*-GaN sample, and (c) a cross-sectional line diagram showing typical variation in the surface potential around a dislocation [90].

is made today in modern EFM, although they used the term *force microscopy of localized charges*). The term *EFM* was coined later, e.g., the study by Sugawara *et al.* [31], who studied the charges localized on the surface in a high vacuum (but, as earlier, they determined the charge sign from the change of the contrast at different  $V_{DC}$  values).

As a matter of fact, it is difficult to rigorously divide the application spheres of the methods—some modern SKPM instruments also provide control for  $\partial C/\partial z$  variation. Thus, the heterodyne system allows one to follow cantilever deflection simultaneously at various frequencies [20, 48, 75] (the cantilever response shows several peaks because the probe behaves as a lumped mass system). If an instrument records only one basic harmonic, one can also measure the capacitance component by tuning the frequency of the applied alternating voltage to  $\omega/2$  [44]. However, the authors of the studies cited above prefer to call their approach Kelvin microscopy. Reciprically, EFM still allows one to compensate the contact potential difference by the Kelvin method, see, e.g., [48], where the potential and capacitance images are compared. However, most often, it is the electrostatic force that is the quantity whose spatial distribution forms an image, as is the case in [31], where the images are obtained based on the force gradient distri-

bution, in [93], where the images are considered in terms of the amplitudes of the  $F_{\omega}$  component, or in [94], where the images are obtained using the  $F_{\omega}$  and  $F_{2\omega}$  amplitudes separately.

Leaving aside the two-pass method [36, 95] and recording the signals simultaneously at several frequencies [48, 94] (Figs. 3 and 4), one has to take into account that the electrostatic force can influence the topographic images. Indeed, the application of the modulating voltage  $V_{AC}\sin\omega t$  makes the constant force component active even at the compensated contact potential difference ( $V_{DC} + V_{CPD} = 0$ ) in accordance with Eq. (2). Although the van der Waals force varies with distance faster than the electrostatic force and it is its gradient  $F'_{vdW}$  that plays the key part in imaging of the constant gradient, the electrostatic-force gradient can also give a contribution. Figure 11 [96] compares the topographic images of the Au sample obtained without application of  $V_{AC}$  and with the application of  $V_{AC} = 10$  V and illustrates how this deteriorates the spatial resolution. It follows from Eqs. (2) and (4) that, in the case where  $V_{CPD} = -V_{DC}$ , the gradient of the constant component of the electrostatic force  $F'_{DC} = 1/4(\partial^2 C/\partial z^2)V_{AC}^2$  coincides (by an absolute value) with

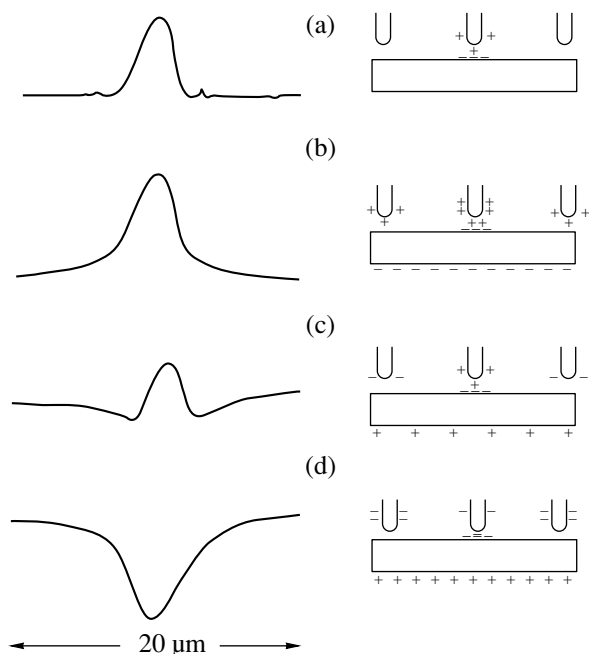


**Fig. 10.** Contours of constant force gradient acting on the tip above the dielectric polymethyl methacrylate surface and the schematic charge distribution at four different applied constant bias voltages: (a) 0, (b) -6, (c) +6, and (d) +24 V [10].

the gradient of the amplitude of the second harmonic of the force  $F'_2 = -1/4(\partial^2 C/\partial z^2)V_{AC}^2$ . Therefore, it was suggested [34, 93] to avoid possible distortions introduced by  $F'_{DC}$  into the topographic images by subtracting the

measured amplitude  $F'_{2\omega}$  from the gradient of the total constant force  $F' = F'_{vdW} + F'_{DC}$ . The dependences of the shift of the frequency of cantilever oscillations (measure of the force gradient) on the height of the tip location above the surface (Fig. 12) [93] demonstrate the practical coincidence of the curve constructed in the absence of the a.c. voltage (filled circles) and the curve constructed for the applied a.c. voltage and then corrected by the above method (open circles).

The authenticity of the topographic image in [31] is ensured in a somewhat different way. It is suggested to apply to a sample square-wave voltage trains with the frequency  $\omega$ . In this case, topographic images are formed in the conventional way at the zero bias (measured from the compensation level of the contact potential difference), whereas the electrostatic characteristics are recorded during the half-period of the bias application.

In turn, Hong *et al.* [46] state that it is possible to overcome the difficulties associated with the separation of the force gradients by using EFM in the dynamic contact mode (dynamic contact mode of EFM, DC-EFM) [97]. It was established that, even in the case of a contact with the solid surface, the cantilever performs continuous oscillations with a finite amplitude. Therefore, the surface profile is measured in the mode analogous to the conventional contact mode in AFM, whereas the electric characteristics are determined from Eqs. (2)–(4) using the oscillation amplitudes at the applied-voltage frequency. In this case, the repulsive van der Waals force is maintained constant with the aid of the feedback in the circuit for the motion control along the vertical coordinate. The above formulas

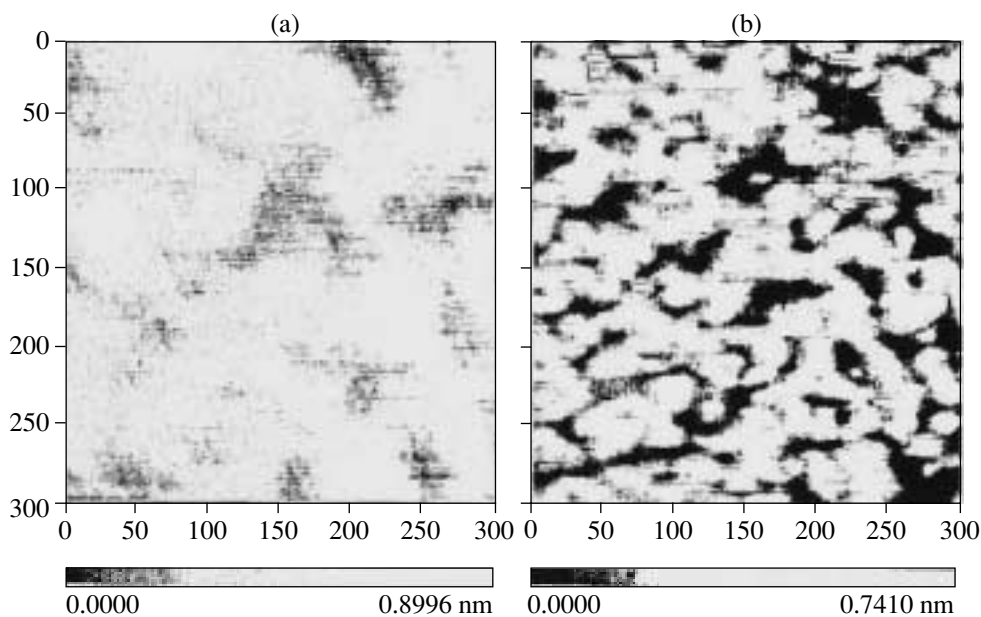


**Fig. 11.** Topography of the surfaces of arachidic acid and partly fluorinated carboxylic acid-based Langmuir–Blodgett films obtained under (a) 10 V and (b) zero a.c. voltage [96].

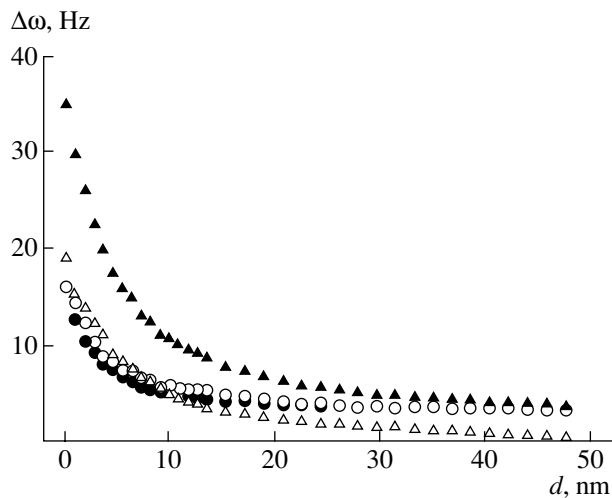


**Fig. 12.** Frequency shift  $\Delta\omega$  as a function of tip height  $d$  above the Si(111) surface under various experimental conditions [93]. ● with no applied voltage; ▲ with an applied 1 V a.c. voltage at frequency  $\omega/2\pi = 300$  Hz; ○ with applied 1 V a.c. voltage after the subtraction from the signal of the component corresponding to the frequency  $2\omega$ ; and △ the signal amplitude at the frequency  $2\omega$ .

remain valid, since, despite, the cantilever contact, no current can flow between the sample and cantilever because of the insulating (oxide) layer on the silicon tip. It is true that, if the samples are insufficiently hard, an additional indeterminate factor arises, which is associated with possible variations in the hardness along the surface changing, in turn, the amplitude of cantilever oscillations (on the other hand, this fact can be used for obtaining some information on the mechanical hardness of the sample) [33].

As to the measurable electric quantities, the directly determined  $F_1$  and  $F_2$  values are insufficiently informative for surface characterization. It is more important to determine the surface potential. In EFM, it is sometimes determined using a Kelvin compensation scheme [48]. It is also possible to determine the surface potential directly from the  $F_1$  and  $F_2$  values using Eqs. (3) and (4),

$$|V_{CPD} + V_{DC}| = V_{AC}/4 |F_1/F_2|. \quad (7)$$

Xu and Hsu proved [94] that the latter method of determining  $V_{CPD}$  is equivalent to the SKPM method even if one takes into account the influence of the stray cantilever–sample capacitance  $C_{cant}$ . Taking into account this capacitance in both methods equally decreases the measured contact potential difference in comparison with its true value because of the coefficient  $\partial C/\partial z / (\partial C/\partial z + \partial C_{cant}/\partial z)$ , amounting in practice to about 85%. Although the determination of  $V_{CPD}$  from  $F_1$  and  $F_2$  requires an additional treatment of the experimental data, it also has an advantage—one can obtain potential images at different bias values  $V_{DC}$ . As is indicated in [94], varying  $V_{DC}$ , it is possible to inverse the

contrast for patches having different work functions. Indeed, consider two patches on the surface with the contact potential difference of the first one,  $V_{CPD1}$ , being higher than for the second one,  $V_{CPD2}$ . Applying a bias  $V_{DC}$  exceeding  $-V_{CPD2}$ , we can make the first patch on the image brighter than the second one (the  $|V_{CPD} + V_{DC}|$  value of this patch is higher). And, vice versa, applying  $V_{DC} < -V_{CPD1}$ , we can make the first patch darker than the second one. Xu and Hsu believe [94] that this can help one to distinguish the true signal of electrostatic origin from the topographic artefacts (the signals at different frequencies were recorded simultaneously). Moreover, analyzing the bias influence (and, first of all, of the bias sign) on the contrast of EFM image with an atomic resolution, Sugawara *et al.* [31] drew conclusions about the sign of a point-defect charge.

The  $F_1/F_2$  ratio is also very useful for studying the character of the electrostatic tip–surface interaction. If the tip and the surface interact as two conductors, then Eq. (7) is valid, with the  $F_1/F_2$  ratio being independent of the tip height above the surface. If semiconductor effects become important, the ratio depends on the tip height [42]. This method suggested in this theoretical study [42] was first used in practice by Sommerhalter *et al.* [44], who verified the validity of the model of conductor interaction for silicon cantilevers.

If a sample is coated with an oxide layer or is an insulator (then, it can be considered as a dielectric interlayer between the lower electrode and the tip), localized charges are formed on the surface. In this case, the force acting on the tip consists not only of the “capacitance component” described by Eq. (1), but one has also to take into account the effect of the field  $E_s$  of surface charges (dependent on the surface charge density  $\sigma$ ) on the induced charge at the tip,  $q_t$ . Information on this density may also be obtained, but in a way more complicated than information about the surface potential [45]. In the dynamic contact EFM [33, 46], the tip is very close to the surface, so that the field of surface charges can be considered to be uniform with the intensity  $\sigma/2\epsilon_0$  (it is assumed that the dimension of the surface-charge region exceeds the apex radius). Introducing an additional contribution  $q_t E_s = C V \sigma / 2 \epsilon_0$  into Eq. (1), we add the term  $C \sigma V_{DC} / 2 \epsilon_0$  to the Eq. (2) for the constant force, while the first harmonic in Eq. (3) is then represented as  $F_\omega = (\partial C / \partial z (V_{CPD} + V_{DC}) + C \sigma / 2 \epsilon_0) V_{AC} \sin \omega t$ . Measuring the first harmonic of the electrostatic force at a constant capacitance, one can determine  $V_{CPD}$  or  $\sigma$  depending on the experimental conditions used. In order to determine  $\sigma$  (e.g., in ferroelectrics), Hong *et al.* [46] suggested using the compensation method as in the case of  $V_{CPD}$ . Using  $V_{DC}$  value such that no signal was recorded at the frequency  $\omega$ , one obtains  $\sigma \sim -2 \epsilon_0 V_{DC} (\partial C / \partial z) / C$ . Taking into account that the sample–surface distance is rather small ( $\sim 1$  nm), the system can be considered as a flat capacitor for which

$(\partial C/\partial z)/C = 1/d$ . This allows one to avoid the necessity of knowing the exact value of the capacitance. The uniform field distribution was used in [98] to take into account the influence of a homogeneous charged contaminated layer on the conducting-sample surface. Saint Jean *et al.* [98] drew the conclusion that the contact potential difference determined by the SKPM method for a surface coated with a contaminated layer of the thickness  $d$  with the dielectric constant  $\epsilon$  and the surface-charge density  $\sigma_s$  is, in fact, the contact potential difference of a clean surface in vacuum with due regard for the additive correction  $\sigma_s d/\epsilon\epsilon_0$ .

However, in the noncontact mode, the problem of determination of the distribution of the surface charges localized in rather small regions cannot be solved correctly under the assumption that the field of charges is uniform. It is more adequate for representing the effect of this field on the tip as an interaction of two point charges spaced by a distance  $z$ —a surface charge  $q_s$  and an induced charge  $q_t$  [12, 36, 40, 93]. Then, the term  $q_s q_t/4\pi\epsilon\epsilon_0 z^2$  (which appears in addition to the capacitance component of the electrostatic force in Eq. (1)) gives the contributions  $q_s^2/4\pi\epsilon\epsilon_0 z^2 + q_s V_{DC}C/4\pi\epsilon\epsilon_0 z^2$  to the constant force component in Eq. (2) and the contribution  $q_s V_{AC}C/4\pi\epsilon\epsilon_0 z^2$  to the first harmonic in Eq. (3) [40]. This results in the modulation of the force gradient at the frequency of the first harmonic used in [12, 92] for obtaining a charge image. Terris *et al.* [12] emphasize a very high sensitivity of the method with respect to the electric charge—the minimum detected value equals three elementary charges. The possible recording of the single-electron processes by this method is confirmed by Schönerberger and Alvarado [99], who studied the relaxation of a charge applied to the surface of a  $\text{Si}_3\text{N}_4$  dielectric. The change in the charge was established from the temporal curve of the first harmonic of the force  $F_\omega$  (with the tip–surface distance and the  $F_{2\omega}$  value being constant), which demonstrated the pronounced signs of quantization. (By the way, the SKPM method also allows one to obtain the screened Coulomb potential of a single charge [70].) According to the estimate made in [29], this charge can be recorded at the tip height of about 15 nm and the dipole moment of 1 D at a distance of 1.5 nm. However, similar studies are still of a qualitative nature [31]. It is important that, in this case, the microscope probe may play not only the passive role (providing the signal forming an image), but also the active one—supplying bias of various values between the cantilever and the substrate, and one may apply to a dielectric film the various charges of different signs. Such recordings can also be made in the noncontact mode (if the voltage pulse is applied with the aid of a crown discharge in the air gap) [92, 99] and also by the contact method [12, 92]. This fact seems to be rather promising for creating memory devices based on ferroelectric materials,

whereas the use of EFM allows one both to record and read the information [100, 101].

Ferroelectric crystals are the first “candidates” for studying their properties by EFM because the method allows one both to visualize domains and to study their dynamics and also give the direct information about their signs, e.g., from the contrast variations at different applied bias voltages [36]. The gradient of the interaction force depends on the magnitude of polarization but not on its sign [102]. Nevertheless, interpretation of the results is not easy, because the contributions to the contrast come not only from the electrostatic but also from the piezoelectric effect, which gives rise to surface vibrations and, finally, to modulations of cantilever oscillations, especially for the first harmonic (electrostriction may also take place, but it gives contributions to higher-order harmonics [103]). Happily, the signal associated with piezoelectricity does not depend on the spring constant of the cantilever, whereas the electrostatic response is inversely proportional to  $k$ . The latter fact allows one to vary the relative contributions of these effects [104]. In turn, the piezoelectric effect may also be studied by EFM, but here one has to take into account the electrostatic interaction. Thus, Durkan *et al.* [105] made it analytically determining the piezoelectric parameters of lead zirconate–titanate. Ni *et al.* [106] studied by EFM the surface polarization of Li-doped ZnO films and revealed the charge of defects induced by the piezoelectric effect.

The possibility of obtaining the images of ferroelectric domains and domain walls by the EFM method at a spatial resolution of 50 nm was demonstrated on  $\text{Gd}_2(\text{MO}_4)_3$  [102]. The nature of the contrast of images of oppositely charged domains and the methodical aspects of their visualization (including the determination of the domain-wall thickness) were analyzed in detail for both noncontact and contact dynamic EFM for triglycine sulfate [104]. Under the conditions of noncontact EFM, the contributions of the electrostatic and piezoelectric effects have the same phases [103], whereas for the contact EFM these effects are in counterphase [100], which simplifies the separation of their contributions. The authors of the contact method [33] state that the contrast of domain images in their experiments is higher than in the noncontact EFM. For a cleaved triglycine sulfate crystal, they manage not only to determine the sign of polarization, but also to calculate the surface-charge density ( $2.7 \mu\text{K}/\text{cm}^2$  at room temperature) by the method described above and to study its change during heating [46]. The polarization switching of domains under pulsed voltage and their further relaxation were also studied in the contact mode [100, 101]. It was established that triglycine sulfate is not an appropriate material for recording information because of its fast return to the initial state (the relaxation time equals 5 min). It is more appropriate to record the information on  $\text{BaTiO}_3$  crystals—the lines are sharper and remain stable for more than five days

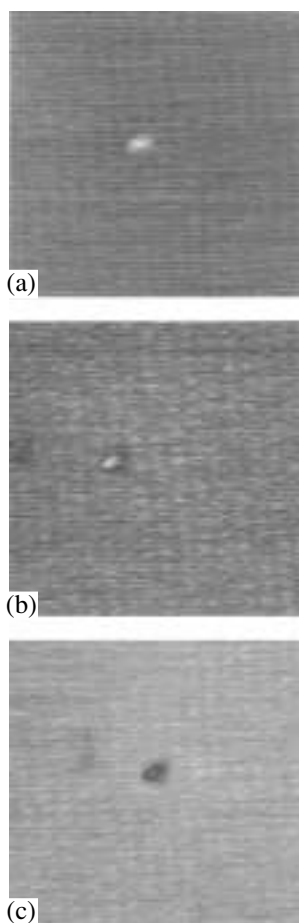


**Fig. 13.** EFM images of the GaAs(110) surface in the vicinity of a point defect at three different bias voltages: (a) +0.5, (b) -0.22, and (c) -0.43 V. Scan size is  $85 \times 85 \text{ \AA}$  [31].

[100]. Using EFM, it is possible to control the spatial-periodic polarization on the surface of  $\text{KTiOPO}_4$  crystals on the nanoscale (“organized” by selective diffusion of rubidium ions) in fields with an intensity exceeding  $750 \text{ V/cm}$  [101].

Using the noncontact mode to guanidinium aluminum sulfate hexahydrate samples, Bluhm *et al.* [36] established that the static EFM variant is preferable for studying the domain structure. The topography of the surface was obtained in the contact mode during the first scanning, whereas during the second scanning, the tip moved at a constant height above the surface and the measure of the electrostatic interaction was the cantilever deflection. This method was also successfully used for studying the domain structure of  $\text{LiNbO}_3$  crystals with polarization-inverted gratings obtained by diffusion of Ti atoms introduced into the structure [107].

The EFM method is also successfully used for solving various problems of microelectronics and, first of all, for defect characterization, e.g., for studying antiphase boundaries on the GaAs/Ge surface [94], point defects on the GaAs surfaces [31] (Fig. 13), and

the relaxation of charges trapped by the  $\text{SiO}_2$  layer on Si substrates [108], with the charge sign being determined by applying various bias voltages. The possibility of using EFM for studying specific defects on the surface was shown in [95]: inversion domains of the N and Ga polarity (the regions with opposite polarizations formed during crystal growth). The quality of the ohmic Au/Ti contacts and the surface conductivity of the epitaxial layer under these contacts in the  $n^+$ -GaInAs/ $n^+$ -InP/InP heterostructure, which simulated a transmission line, were determined in [109]. Using EFM, Girard *et al.* [110] observed self-organization of InAs islands on the GaAs(001) surface. Ankudinov *et al.* [111] compared the electric parameters of the laser *pin*-diode based on the AlGaAs/GaAs heterostructure obtained by the noncontact and contact dynamic EFM methods and revealed no considerable differences. They only state that the contact mode allows one to attain a slightly higher spatial sensitivity at the atomic level, whereas the noncontact mode allows one to attain the admissible signal/noise ratio at a lower  $V_{AC}$  value.

Considering various EFM applications, one must mention the studies of organic objects examined by this method from the very beginning. Thus, Terris *et al.* [12] visualized the distribution of charges localized on the polymethyl methacrylate (PMMA) surface. The recent studies along this direction are based on the direct measurement of the potential by the SKM method. For organic and biological objects whose properties are determined by polar functional groups ( $-\text{OH}$ ,  $-\text{COOH}$ ,  $-\text{NH}_2$ , etc.), the surface potential is closely related to their functions. Knowing the distribution of the surface potential at the molecular resolution, it is possible to extract detailed information on various complicated chemical processes. Thus, today, it is possible to recognize the regions containing the thiol molecules with chemically different terminal head groups [112], determine the local distribution of the doping (oxidation) level of polymer films (polybithiophene [113, 114]), and analyze the polarization distribution in polymer films (polymethyl methacrylate with 10% chromophore [115]). Thus, one can obtain the necessary information on the homogeneity and domain structure of Langmuir–Blodgett films of various compositions (e.g., experiments on films based on the behenic and perfluorotetradecanoic acids with calcium cations [116], orientation of amphiphilic molecules in multilayer films (experiments with cadmium arachidate [117]), the site of localization of contamination on the surface or under the film on the substrate (experiment with films based on the arachidic and partially fluorinated carboxylic acids [96]), etc. The EFM data allow one to draw some conclusions on the particle boundaries in the poly(styrene-butyl acrylate-acrylic acid) latex films [118], on the electric conductivity of DNA molecules [119] and complexes of these molecules with metal ions [120] and the interaction of DNA molecules with substrates [121]. Similar data should also

be very useful in the study of the electron structure of porphyrines [122] and photoprocesses occurring with their participation on the surface [123] and also in the search for physiologically active substances in cells in immunohistochemical reactions [124].

## 5. SCANNING CAPACITANCE MICROSCOPY

It is seen from what has been stated above that the relation between the electrostatic force and capacitance allows one to determine the latter. This can be realized by the EFM on the basis of Eq. (4). This was done first by Martin *et al.* [8], who measured the minimum detectable capacitance as  $4 \times 10^{-20}$  F using a constant bias voltage (the capacitance was calculated for a model of flat capacitor or a sphere above the plane with the measured force gradient) and as  $8 \times 10^{-22}$  F using the modulation method (with the separation of the signal at the second harmonic for the same cantilever-sample models). Geometric modeling of the system is dictated here by the fact that, in this case, one controls experimentally not the capacitance itself but its derivative  $\partial C/\partial z$  described by Eq. (4). The direct measurement of capacitance can be made by the method of scanning capacitance microscopy (SCM) developed independently of the force methods of recording.

The first scanning capacitance microscope [13] was constructed earlier than the atomic force microscope and used another scanning system based on the scanning RCA videodisk system. The measuring probe was a thin-film vertical electrode with the cross section  $0.1 \times 2.0 \mu\text{m}$  deposited onto a diamond tip and ending 20 nm from its base. The tip, brought into mechanical contact with the sample surface, moved along the spiral, and the capacitance of the electrode-sample system was recorded during this motion by an RCA capacitance sensor. The signal was digitally processed and formed the surface image. It is interesting that the first problem solved by the SCM method was visualization of topography. Considering the changes in the capacitance value, one can extract the information on the probe height above the surface. The next scanning capacitance microscope was designed with the same goal [16]. The probe was a thin metal wire, the spiral scanning was changed to linear scanning performed due to motion of the sample with respect to the probe in the surface plane along two mutually perpendicular directions. The capacitance was controlled by an LCR resonance circuit-based sensor, which included the capacitance to be determined. The probe-surface distance was controlled using feedback in such a way that the signal would remain constant. The heights thus obtained formed the image, i.e., allowed one to obtain the contours of constant capacitance (or, more exactly, differential capacitance, because the piezoelectric holder provided sinusoidal modulation of the probe-sample distance, which ensured a high degree of locality of the information obtained). It was assumed that the

images thus obtained are directly related to the topography of the surface, although it was also indicated that the images were also dependent on the inhomogeneities of the electric characteristics of the sample. The possibility of obtaining information on the electric properties of the sample in such a way (dielectric constant or the shape of ferroelectric domains) was still indicated in [13].

It was only later that the capacitance value started playing the important role. This happened when an RCA-sensor-based capacitance microscope began using the scanning system and the feedback of a scanning tunneling microscope [125]. This allowed one to independently control also the surface relief (in this study it was reconstructed from the values of the tunneling current) and the capacitance, which could serve as a source of additional information [126]. Williams *et al.* [125] evaluated the minimum recordable capacitance value as  $2 \times 10^{-22}$  F, with the best signal/noise ratio being obtained for the differential capacitance measured by modulating the probe-sample distance. However, in the new modification of the instrument, capacitance first played the auxiliary role, being a component of an electrical oscillating contour and the control system of cantilever deflection [127]. In other words, it was used to determine the force acting on the cantilever, e.g., the magnetic force [128]. Sarid [40] discussed the possible use of capacitance created not by the probe-sample system, but by the probe-special reference plate one. However, the capacitance related to the given sample region can be very informative. This new function (measurement of the capacitance with the aid of an RCA-sensor-based circuit with the sensitivity  $10^{-19}$  F) was used to increase the possibilities of the atomic force microscope with a metallized probe [129]. Thus, the  $C(V)$  curves for the metal-dielectric-semiconductor structure were obtained at high frequencies ( $>1$  kHz). If the dielectric layer is charged, then the field of its charges acts as an additional bias at the capacitor and the  $C(V)$  curve shifts along the abscissa. This phenomenon can readily be recorded using the  $dC(V)/dV$  curves. At the same time, the microscope was used not only for observations but also for recording the information [129, 130]. Applying the pulses of pronounced bias, it was possible to inject charges into the insulating layer locally, where they remained trapped for quite a long time. The record could be erased by applying a voltage pulse of opposite polarity.

Today, a scanning capacitance microscope is an atomic-force microscope equipped with a highly sensitive capacitance sensor usually operating at a frequency of 915 MHz. Its signal is recorded in parallel with the topographic signal [131]. Thus, one can obtain the topographic image of the surface (as usual, measuring cantilever deflections) and, simultaneously, also the distribution of the capacitance over the surface. The sensor is an oscillatory circuit including the capacitance of the sample-electrode system and is excited by a UHF source (Fig. 14). The changes in this capacitance

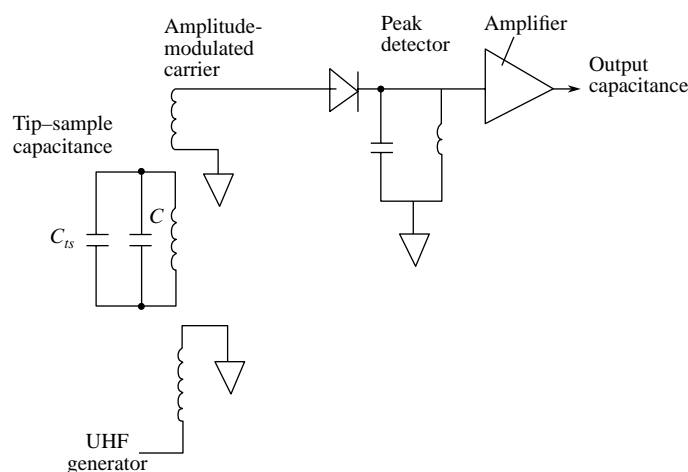


Fig. 14. Schematic of an RCA capacitance sensor.

lead to the shift of the resonance frequency of the circuit; then, the oscillation amplitude varies, which is recorded by a peak detector. At present, designers are attempting to increase the sensitivity of the capacitance part of the circuit. Thus, the sensitivity of a modified instrument demonstrated at the 11th International conference on scanning tunneling microscopy in Vancouver, Canada, in July, 2001 [132], was 30 times higher than the sensitivity of a standard RCA attachment. This was attained by thorough screening of the active components from stray fields in the probe region by using special technical innovations. It was also suggested to use the microscope in the mode of “shear forces,” when the probe oscillations are excited electromechanically in the surface plane along the scanning direction [133]. In this case, it is possible to record simultaneously the topographic image and the distribution of the  $dC/dV$  and  $dC/dx$  quantities (where  $x$  is the coordinate along the surface). Also, the probe technique is developed, which allows one to make measurements at different temperatures [134], including temperatures as low as 1.5 K [135]. The theoretical methods for calculating capacitance of the surfaces with arbitrary profiles have also been developed [136].

Following the classical macroscopic method of determining the doping level of a semiconductor based on the  $C(V)$  dependence, scanning capacitance microscopy also became the standard method for control of two-dimensional dopant distributions in microelectronic devices [137]. In fact, the accuracy of the information thus obtained considerably depends on the adequacy of the models used in data interpretation. The possibility of establishing the distribution of impurity along the surface from the measured  $F(V)$  dependences was predicted theoretically in [43] for the simplest plane-parallel geometry of the tip–vacuum gap–oxide–semiconductor system. It was shown that it is better to use the  $F_{\omega}(V)$  and  $F_{2\omega}(V)$  dependences than the  $F_{DC}(V)$

dependence. Soon, the use of SCM made it possible to directly measure the capacitance as a function of voltage for  $n$ -Si wafers homogeneously doped to different levels. The doping level was evaluated for each wafer (with the tip being in contact with the oxide layer) [138]. Then, detailed theoretical computations were made for the tips of some configurations by both analytical [139, 140] and numerical [141, 142] methods based on the solution of the Poisson equation for a semiconductor. This allowed one to relate the capacitance value  $C(V)$  or  $dC/dV$  to the concentration of electrically active impurity atoms at the given point. These computations were complemented with the comparison of the experimental SCM data for the test structure (e.g., cross sections of silicon  $p^+/p$  structure,  $p$ - $n$ -junctions [143] and  $n^+/n$  structures [144, 145], and also the Si/Ge system [146]) with the results obtained by secondary ion-mass spectroscopy (SIMS). It became possible to increase the method sensitivity by preparing the samples for the studies in different ways, e.g., by surface bevelling [147–149]. At present, the theoretical basis of the method is being developed for various experimental situations. In particular, analysis showed [150] that the capacitance value is controlled by the macroscopic geometry of the tip, rather than by the sample parameters, and therefore these parameters should be determined using  $dC/dV$ .

Methodically, it is simpler to measure the  $dC/dV$  derivative than the absolute capacitance value (in this case, the effect of a considerable stray capacitance is excluded and the signal/noise ratio increases). However, Tomiye and Yao [151] believe that this may give rise to an additional problem associated with the effect of the  $V_{AC}$  value. On the contrary, Stephenson *et al.* [152] believe that a  $V_{AC}$  value not exceeding 0.2–0.4 V does not influence the results, whereas the latter can be dependent, to some extent, on the bias voltage. In order to record the  $dC/dV$  curve using a capacitance sensor of

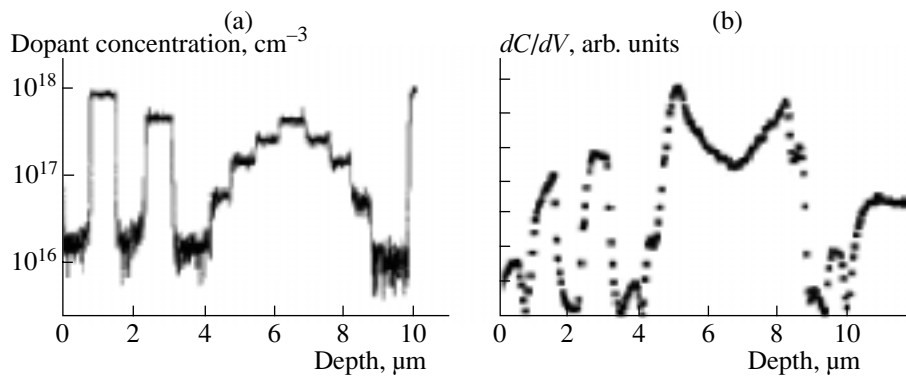


**Fig. 15.** (a) SIMS profile of nitrogen concentration in the epitaxial  $n$ -type structure and (b) the differential-capacitance profile of the same sample ( $V_{AC} = 1$  V and  $V_{DC} = -4$  V) [155].

a microscope, in addition to the bias voltage varying within  $-10$ – $+10$  V, one has also to supply a modulating voltage with the amplitude  $\leq 1$  V and the frequency 5–20 kHz and to record the corresponding capacitance change. Another variant of the method is based on the feedback with respect to the variable voltage: the  $V_{AC}$  value is chosen in such a way that the variation in the capacitance  $dC$  during the whole scanning cycle remains constant and one records the  $dV/dC$  values [143, 153]. The results obtained can readily be recalculated into the value of the doping level using the database containing calibration curves calculated by the finite-element method for various doping levels and thicknesses of the oxide layer and the specially designed software [141]. The algorithm suggested here is valid in the case in which the gradient of the doping level is not too high. The limitations associated with this condition are analyzed in detail elsewhere [154] (the rate of the variation of the impurity concentration along the surface should be related in a certain way with the tip diameter).

However, leaving aside the requirements set by the quantitative interpretation of the results, the SCM method allows one to obtain the contrast from doped regions of nanometer sizes as in the case of silicon plates subjected to ion implantation through a mask [153]. In fact, the  $dC/dV$  values themselves turn out to be rather informative (Fig. 15, where the curve constructed for the cross section of the epitaxial structure consisting of alternating  $n$ - (nitrogen-doped) and  $p$ - (trimethylaluminum-doped) SiC layers neighbors the concentration profile found by SIMS [155]). An example of the quantitative treatment of the  $dC/dV$  dependences is illustrated by Fig. 16 [156], which presents the concentration profiles of the majority carriers in the cross section of the  $N^+$ -implanted 6H-SiC sample obtained by such a method.

In addition to characterization of the  $p$ - $n$  junctions [151, 157–161], scanning capacitance microscopy is also used for studying the charging effect in  $Al_xGa_{1-x}N/GaN$  heterostructures [162, 163] and  $SiO_2$

layers on Si substrates [164, 165], compensation of shallow donor levels in Fe-doped InP [166], ordering in the GaInP sample [167, 168], dislocations in GaN [169], surface depletion at quantum InAs dots on GaAs [170], and comparison of  $SiO_2$  layers obtained by various methods of oxidation [171].

One often invokes as additional information the data on the spatial capacitance distribution in EFM and SKPM studies (in this case, the  $dC/dz$  value is recorded). This allows one to determine the dopant profiles [20, 172], analyze the defects in GaAs/Ge [94], etc. Kimura *et al.* [173] suggested taking into account the  $C(V)$  dependence arising in semiconductors by using an approximate method under the assumption

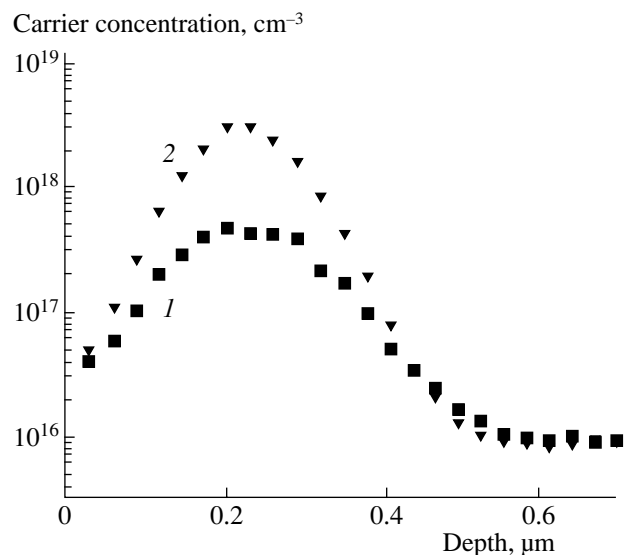


**Fig. 16.** Carrier concentration profiles measured at room temperature by the SCM method on 200-keV  $N^+$ -implanted 6H-SiC samples at two different fluences: (1)  $1 \times 10^{14}$  and (2)  $5 \times 10^{14}$   $cm^{-2}$  [156].

that we have, in Eq. (1),

$$\partial C/\partial z \approx \partial C(V_{DC}, z)/\partial z + \partial^2 C(V_{DC}, z)/\partial z \partial V_{AC} \sin \omega t.$$

Then, the signal acquires a periodic component corresponding to the third harmonic at  $3\omega$  proportional to  $\partial^2 C/\partial z \partial V$ , which yields the information on  $\partial C/\partial V$ . Experiments with the test doped *n*- and *p*-type Si samples confirmed that this method can be used for determining two-dimensional doping profiles, with the contrast in the vicinity of the *p-n* junction being dependent on the  $V_{DC}$  value [173].

Scanning probe microscopy is a rapidly developing method of studying processes on the molecular scale. The theoretical foundations of the method are constantly being refined and the experimental methods are becoming more elaborate. Although the number of papers using this method is increasing in a flood, there still are fields for its new application. There is no doubt that we shall witness numerous interesting discoveries in this field.

#### ACKNOWLEDGMENTS

This study was supported by the Vainshtein Scientific School on Dynamical and Kinematical Scattering of X-rays and Electrons (Theory, Experimental Methods, and Applications), project NSH-1404.2003.2.

#### REFERENCES

- G. Binnig, C. F. Quate, and Ch. Gerber, *Phys. Rev. Lett.* **56**, 930 (1986).
- Y. Martin and H. K. Wickramasinghe, *Appl. Phys. Lett.* **50**, 1455 (1987).
- J. J. Sáenz, N. Garcia, P. Grütter, *et al.*, *J. Appl. Phys.* **62**, 4293 (1987).
- A. Wadas, *J. Magn. Magn. Mater.* **71**, 147 (1988).
- U. Hartmann, *J. Appl. Phys.* **64**, 1561 (1988).
- J. Sáenz, N. Garcia, and J. C. Slonczewski, *Appl. Phys. Lett.* **53**, 1449 (1988).
- M. Mansuripur, *IEEE Trans. Magn.* **25**, 3467 (1989).
- Y. Martin, D. W. Abraham, and H. K. Wickramasinghe, *Appl. Phys. Lett.* **52**, 1103 (1988).
- R. Erlandsson, G. M. McClelland, C. M. Mate, and S. Chiang, *J. Vac. Sci. Technol. A* **6**, 266 (1988).
- J. E. Stern, B. D. Terris, H. J. Mamin, and D. Rugar, *Appl. Phys. Lett.* **53**, 2717 (1988).
- C. Schönenberger and S. F. Alvarado, *Rev. Sci. Instrum.* **60**, 3131 (1989).
- B. D. Terris, J. E. Stern, D. Rugar, and H. J. Mamin, *Phys. Rev. B* **63**, 2669 (1989).
- J. R. Matey and J. Blanc, *J. Appl. Phys.* **57**, 1437 (1985).
- I. V. Yaminskiĭ and A. M. Tishin, *Usp. Khim.* **68** (3), 187 (1999).
- S. Lányi, J. Török, and P. Řehůřek, *Rev. Sci. Instrum.* **65**, 2258 (1994).
- C. D. Bugg and P. J. King, *J. Phys. E: Sci. Instrum.* **21**, 147 (1988).
- J. L. de Jong and J. D. Reimer, *Scan. Electron Microsc.* **3**, 933 (1986).
- P. Muralt and D. W. Pohl, *Appl. Phys. Lett.* **48**, 514 (1986).
- J. P. Pelz and R. H. Koch, *Rev. Sci. Instrum.* **60**, 301 (1989).
- A. K. Henning, T. Hochwitz, J. Slinkman, *et al.*, *J. Appl. Phys.* **77**, 1888 (1995).
- U. Hartmann, *Ultramicroscopy* **42–44**, 59 (1992).
- O. Teschke and E. F. de Souza, *Appl. Phys. Lett.* **74**, 1755 (1999).
- Y. Martin, C. C. Williams, and H. K. Wickramasinghe, *J. Appl. Phys.* **61**, 4723 (1987).
- H. W. Hao, A. M. Baró, and J. J. Sáenz, *J. Vac. Sci. Technol. B* **9**, 1323 (1991).
- S. Gómez-Moñivas, L. S. Froufe-Pérez, A. J. Caamaño, and J. J. Sáenz, *Appl. Phys. Lett.* **79**, 4048 (2001).
- S. Belaidi, F. Lebon, P. Girard, *et al.*, *Appl. Phys. A* **66**, S239 (1998).
- S. Belaidi, P. Girard, and G. Lévêque, *J. Appl. Phys.* **81**, 1023 (1997).
- S. Belaidi, P. Girard, and G. Lévêque, *Microelectron. Reliab.* **37**, 1627 (1997).
- D. M. Taylor, *Thin Solid Films* **331**, 1 (1998).
- A. Gil, J. Colchero, J. Gómez-Herrero, and A. M. Baró, *Nanotechnology* **14**, 332 (2003).
- Y. Sugawara, T. Uchihashi, M. Abe, and S. Morita, *Appl. Surf. Sci.* **140**, 371 (1999).
- S. Sounilhac, E. Barthel, and F. Creuzet, *Appl. Surf. Sci.* **140**, 411 (1999).
- J. W. Hong, S.-I. Park, and Z. G. Khim, *Rev. Sci. Instrum.* **70**, 1735 (1999).
- K. Okamoto, Y. Sugawara, and S. Morita, *Appl. Surf. Sci.* **188**, 381 (2002).
- S. Gómez-Moñivas, L. S. Froufe, R. Carminati, *et al.*, *Nanotechnology* **12**, 496 (2001).
- H. Bluhm, A. Wadas, R. Wiesendanger, *et al.*, *Phys. Rev. B* **55**, 4 (1997).
- A. San Paulo and R. Garcia, *Phys. Rev. B* **66**, 041406(R) (2002).
- S. Kitamura, K. Suzuki, and M. Iwatsuki, *Appl. Surf. Sci.* **140**, 265 (1999).
- S. Kitamura, K. Suzuki, M. Iwatsuki, and C. B. Mooney, *Appl. Surf. Sci.* **157**, 222 (2000).
- D. Sarid, *Scanning Force Microscopy with Applications to Electric, Magnetic, and Atomic Forces* (Oxford Univ. Press, New York, 1994).
- C. Donolato, *J. Appl. Phys.* **78**, 684 (1995).
- S. Hudlet, M. Saint Jean, B. Roulet, *et al.*, *J. Appl. Phys.* **77**, 3308 (1995).
- Y. J. Huang, J. Slinkman, and C. C. Williams, *Ultramicroscopy* **42–44**, 298 (1992).
- Ch. Sommerhalter, Th. Glatzel, Th. W. Matthes, *et al.*, *Appl. Surf. Sci.* **157**, 263 (2000).
- P. Girard, *Nanotechnology* **12**, 485 (2001).
- J. W. Hong, D. S. Kahng, J. C. Shin, *et al.*, *J. Vac. Sci. Technol. B* **16**, 2942 (1998).
- S. Gómez-Moñivas, J. J. Sáenz, R. Carminati, and J. J. Greffet, *Appl. Phys. Lett.* **76**, 2955 (2000).

48. F. Muller, A. D. Muller, M. Hietschold, and S. Kammer, *Meas. Sci. Technol.* **9**, 734 (1998).
49. S. J. T. Van Noort, K. O. Van der Werf, B. G. de Grooth, *et al.*, *Ultramicroscopy* **69**, 117 (1997).
50. J. P. Spatz, S. Sheiko, M. Moller, *et al.*, *Langmuir* **13**, 4699 (1997).
51. R. Hillenbrand, M. Stark, and R. Guckenberger, *Appl. Phys. Lett.* **76**, 3478 (2000).
52. S. J. O'Shea, R. M. Atta, and M. E. Welland, *Rev. Sci. Instrum.* **66**, 2508 (1995).
53. H. O. Jacobs, H. F. Knapp, and A. Stemmer, *Rev. Sci. Instrum.* **70**, 1756 (1999).
54. M. C. Hersam, A. C. F. Hoole, S. J. O'Shea, and M. E. Welland, *Appl. Phys. Lett.* **72**, 915 (1998).
55. A. Efimov and S. R. Cohen, *J. Vac. Sci. Technol. A* **18**, 1051 (2000).
56. T. Trenkler, T. Hantschel, R. Stephenson, *et al.*, *J. Vac. Sci. Technol. B* **18**, 418 (2000).
57. A. Kikukawa, S. Hosaka, and R. Imura, *Appl. Phys. Lett.* **66**, 3510 (1995).
58. T. R. Albrecht, P. Grütter, D. Horne, and D. Rugar, *J. Appl. Phys.* **69**, 668 (1991).
59. S. Kitamura and H. Iwatsuki, *Appl. Phys. Lett.* **72**, 3154 (1998).
60. K. Okamoto, K. Yoshimoto, Y. Sugawara, and S. Morita, *Appl. Surf. Sci.* **210**, 128 (2003).
61. S. Yee, M. Stratmann, and R. A. Oriani, *J. Electrochem. Soc.* **138**, 55 (1991).
62. I. Baikie, U. Peterman, and B. Lagel, *Surf. Sci.* **433–435**, 249 (1999).
63. B. Lagel, I. Baikie, and U. Petermann, *Surf. Sci.* **433–435**, 622 (1999).
64. W. Teliëps and E. Bauer, *Ultramicroscopy* **17**, 57 (1985).
65. B. Bhushan and A. V. Goldade, *Appl. Surf. Sci.* **157**, 373 (2000).
66. J. M. R. Weaver and D. W. Abraham, *J. Vac. Sci. Technol. B* **9**, 1559 (1991).
67. M. Nonnenmacher, M. P. O'Boyle, and H. K. Wickramasinghe, *Appl. Phys. Lett.* **58**, 2921 (1991).
68. M. P. O'Boyle, T. T. Hwang, and H. K. Wickramasinghe, *Appl. Phys. Lett.* **74**, 2641 (1999).
69. B. Bhushan and A. V. Goldade, *Wear* **244**, 107 (2000).
70. Ch. Sommerhalter, Th. W. Matthes, Th. Glatzel, *et al.*, *Appl. Phys. Lett.* **75**, 286 (1999).
71. N. A. Burnham, R. J. Colton, and H. M. Pollock, *Phys. Rev. Lett.* **69**, 144 (1992).
72. H. O. Jacobs, P. Leuchtmann, O. J. Homan, and A. Stemmer, *J. Appl. Phys.* **84**, 1168 (1998).
73. S. Sadewasser, Th. Glatzel, R. Shikler, *et al.*, *Appl. Surf. Sci.* **210**, 32 (2003).
74. O. Vatel and M. Tanimoto, *J. Appl. Phys.* **77**, 2358 (1995).
75. Y. Leng, C. C. Williams, L. C. Su, and G. B. Stringfellow, *Appl. Phys. Lett.* **66**, 1264 (1995).
76. A. K. Henning and T. Hochwitz, *Mater. Sci. Eng. B* **42**, 88 (1996).
77. Th. Glatzel, S. Sadewasser, and M. Ch. Lux-Steiner, *Appl. Surf. Sci.* **210**, 84 (2003).
78. T. Takahashi and T. Kawamukai, *Ultramicroscopy* **82**, 63 (2000).
79. R. Shikler and Y. Rosenwaks, *Appl. Surf. Sci.* **157**, 256 (2000).
80. S. Akita, S. Takahashi, and Y. Nakayama, in *Abstracts of 11th International Conference of Scanning Tunneling Microscopy, Spectroscopy, and Related Techniques* (Vancouver, Canada, 2001), p. 251.
81. S. Ono, M. Takeuchi, and T. Takahashi, *Appl. Phys. Lett.* **78**, 1086 (2001).
82. M. Nonnenmacher, M. O. O'Boyle, and H. K. Wickramasinghe, *Ultramicroscopy* **42–44**, 268 (1992).
83. S. Lévéque, P. Girard, E. Skouri, and D. Yarekha, *Appl. Surf. Sci.* **157**, 251 (2000).
84. A. Sasahara, H. Uetsuka, and H. Onishi, *Surf. Sci.* **529**, L245 (2003).
85. P. Campestrini, E. P. M. van Westing, H. W. van Rooijen, and J. H. W. de Wit, *Corros. Sci.* **42**, 1853 (2000).
86. M. Tanimoto and O. Vatel, *J. Vac. Sci. Technol. B* **14**, 1547 (1996).
87. F. Robin, H. Jakobs, O. Homan, *et al.*, *Appl. Phys. Lett.* **76**, 2907 (2000).
88. A. Breymesser, V. Schlosser, D. Pieró, *et al.*, *Sol. Energy Mater. Sol. Cells* **66**, 171 (2001).
89. R. Shikler, T. Meoded, N. Fried, and Y. Rosenwaks, *Appl. Phys. Lett.* **74**, 2972 (1999).
90. G. Koley and M. G. Spencer, *Appl. Phys. Lett.* **78**, 2873 (2001).
91. M. Vogel, B. Stein, H. Pettersson, and K. Karrai, *Appl. Phys. Lett.* **78**, 2592 (2001).
92. B. D. Terris, J. E. Stern, D. Rugar, and H. J. Mamin, *J. Vac. Sci. Technol. A* **8**, 374 (1990).
93. T. Ishihashi, M. Ohta, Y. Sugawara, *et al.*, *J. Vac. Sci. Technol. B* **15**, 1543 (1997).
94. Q. Xu and J. W. P. Hsu, *J. Appl. Phys.* **85**, 2465 (1999).
95. K. M. Jones, P. Visconti, F. Yun, *et al.*, *Appl. Phys. Lett.* **78**, 2497 (2001).
96. M. Yasutake, D. Aoki, and M. Fujihira, *Thin Solid Films* **273**, 279 (1996).
97. J. W. Hong, G. H. Noh, S. I. Park, *et al.*, *Phys. Rev. B* **58**, 5078 (1998).
98. M. Saint Jean, S. Hudlet, C. Güthmann, and J. Berger, *Phys. Rev. B* **56**, 15391 (1997).
99. C. Schönenberger and S. F. Alvarado, *Phys. Rev. Lett.* **65**, 3162 (1990).
100. L. M. Eng, M. Abplanalp, and P. Günter, *Appl. Phys. A* **66**, S679 (1998).
101. L. M. Eng, J.-H. Güntherodt, G. Rosenman, *et al.*, *J. Appl. Phys.* **83**, 5973 (1998).
102. F. Saurenbach and B. D. Terris, *Appl. Phys. Lett.* **56**, 1703 (1990).
103. K. Franke, *Ferroelectr. Lett. Sect.* **19**, 25 (1995).
104. M. Labardi, V. Likodimos, and M. Allegrini, *Phys. Rev. B* **61**, 14390 (2000).
105. C. Durkan, D. P. Chu, P. Migliorato, and M. E. Welland, *Appl. Phys. Lett.* **76**, 366 (2000).
106. H. Q. Ni, Y. F. Lu, Z. Y. Liu, *et al.*, *Appl. Phys. Lett.* **79**, 812 (2001).

107. H. Bluhm, A. Wadas, R. Wiesendanger, *et al.*, *Appl. Phys. Lett.* **71**, 146 (1997).
108. G. H. Buh, H. J. Chung, and Y. Kuk, *Appl. Phys. Lett.* **79**, 2010 (2001).
109. J. F. Bresse and S. Blayac, *Solid-State Electron.* **45**, 1071 (2001).
110. P. Girard, A. N. Titkov, M. Ramonda, *et al.*, *Appl. Surf. Sci.* **201**, 1 (2002).
111. A. Ankudinov, V. Marushchak, A. Titkov, *et al.*, *Phys. Low-Dimens. Semicond. Struct.* **3–4**, 9 (2001).
112. J. Lu, E. Delamarche, R. Bennewitz, *et al.*, in *Proceedings of 10th International Conference on STM/PPM* (Seoul, 1999), p. 525.
113. O. A. Semenikhin, L. Jiang, T. Iyoda, *et al.*, *Phys. Chem.* **100**, 18603 (1996).
114. O. A. Semenikhin, L. Jiang, T. Iyoda, *et al.*, *Electrochim. Acta* **42**, 3321 (1997).
115. R. Blum, A. Ivankov, S. Schwantes, and M. Eich, *Appl. Phys. Lett.* **76**, 604 (2000).
116. K. Yagi and M. Fujihira, *Appl. Surf. Sci.* **157**, 405 (2000).
117. M. Fujihira and H. Kawate, *J. Vac. Sci. Technol. B* **12**, 1604 (1994).
118. A. J. Keslerek, K. A. R. Costa, and F. Galembeck, *Langmuir* **17**, 7886 (2001).
119. A. Gil, P. J. de Pablo, J. Colchero, *et al.*, *Nanotechnology* **13**, 309 (2002).
120. F. Moreno-Herrero, P. Herrero, F. Moreno, *et al.*, *Nanotechnology* **14**, 128 (2003).
121. K. J. Kwak, S. Yoda, and M. Fujihira, *Appl. Surf. Sci.* **210**, 73 (2003).
122. C. Di Natale, C. Goletti, R. Paolesse, *et al.*, *Sens. Actuators B* **57**, 183 (1999).
123. E. Moons, A. Goossens, and T. Savenije, *J. Phys. Chem. B* **101**, 8492 (1997).
124. S. Yamashina and M. Shigeno, *J. Electron Microsc.* **44**, 462 (1995).
125. C. C. Williams, W. P. Hough, and S. A. Rishton, *Appl. Phys. Lett.* **55**, 203 (1989).
126. Š. Lányi, J. Török, and P. Řehůřek, *J. Vac. Sci. Technol.* **14**, 892 (1996).
127. G. Neubauer, S. R. Cohen, G. M. McClelland, *et al.*, *Rev. Sci. Instrum.* **61**, 1884 (1990).
128. T. Goddenhenrich, H. Lemke, U. Hartmann, and C. Heiden, *J. Vac. Sci. Technol. A* **8**, 383 (1990).
129. R. C. Barret and C. F. Quate, *J. Appl. Phys.* **70**, 2725 (1991).
130. R. C. Barret and C. F. Quate, *Ultramicroscopy* **42–44**, 262 (1992).
131. N. Nakagiri, T. Yamamoto, H. Sugimura, and Y. Suzuki, *J. Vac. Sci. Technol. B* **14**, 887 (1996).
132. P. Stopford, T. Lodhi, R. Elgaid, *et al.*, in *Abstracts of 11th International Conference of Scanning Tunneling Microscopy, Spectroscopy, and Related Techniques* (Vancouver, Canada, 2001), p. 354.
133. Y. Naitou and N. Ookubo, *Appl. Phys. Lett.* **78**, 2955 (2001).
134. C. K. Kim, I. T. Yoon, Y. Kuk, and H. Lim, *Appl. Phys. Lett.* **78**, 613 (2001).
135. X. Yu, F. D. Callaghan, P. J. Moriarti, *et al.*, in *Abstracts of 11th International Conference of Scanning Tunneling Microscopy, Spectroscopy, and Related Techniques* (Vancouver, Canada, 2001), p. 40.
136. A. Garcia-Valenzuela, N. C. Bruce, and D. Kouznetsov, *Appl. Phys. Lett.* **77**, 2066 (2000).
137. A. Born and R. Wiesendanger, *Appl. Phys. A* **66**, 421 (1998).
138. Y. Huang and C. C. Williams, *J. Vac. Sci. Technol. B* **12**, 369 (1994).
139. Y. Huang, C. C. Williams, and J. Slinkman, *Appl. Phys. Lett.* **66**, 344 (1995).
140. C. Donolato, *Mater. Sci. Eng. B* **42**, 99 (1996).
141. J. F. Marchiando, J. J. Kopanski, and J. R. Lowney, *J. Vac. Sci. Technol. B* **16**, 463 (1998).
142. C. C. Williams, *Annu. Rev. Mater. Sci.* **29**, 471 (1999).
143. J. J. Kopanski, J. F. Marchiando, D. W. Benning, *et al.*, *J. Vac. Sci. Technol. B* **16**, 339 (1998).
144. J. S. McMurray, J. Kim, C. C. Williams, and J. Slinkman, *J. Vac. Sci. Technol. B* **16**, 344 (1998).
145. J. Kim, J. S. McMurray, C. C. Williams, and J. Slinkman, *J. Appl. Phys.* **84**, 1305 (1998).
146. Y. Huang, C. C. Williams, and M. A. Wendman, *J. Vac. Sci. Technol. A* **14**, 1168 (1996).
147. F. Giannazzo, F. Priolo, V. Raineri, and V. Privitera, *Appl. Phys. Lett.* **76**, 2565 (2000).
148. F. Giannazzo, V. Raineri, V. Privitera, and F. Priolo, *Mater. Sci. Semicond. Process.* **4**, 77 (2001).
149. L. Ciampolini, F. Giannazzo, M. Ciappa, *et al.*, *Mater. Sci. Semicond. Process.* **4**, 85 (2001).
150. A. Shik and H. E. Ruda, *Surf. Sci.* **532–535**, 1132 (2003).
151. H. Tomiye and T. Yao, *Appl. Surf. Sci.* **159–160**, 210 (2000).
152. R. Stephenson, A. Verhulst, P. de Wolf, *et al.*, *J. Vac. Sci. Technol. B* **18**, 405 (2000).
153. T. Winzell, S. Anand, I. Maximov, *et al.*, *Nucl. Instrum. Methods Phys. Res. B* **173**, 447 (2001).
154. J. F. Marchiando, J. J. Kopanski, and J. Albers, *J. Vac. Sci. Technol. B* **18**, 414 (2000).
155. O. Bowallius, A. Anand, N. Nordell, *et al.*, *Mater. Sci. Semicond. Process.* **4**, 209 (2001).
156. F. Giannazzo, L. Calcagno, F. Roccaforte, *et al.*, *Appl. Surf. Sci.* **184**, 183 (2001).
157. H. Edwards, R. McGlothlin, R. San Martin, *et al.*, *Appl. Phys. Lett.* **72**, 698 (1998).
158. M. L. O'Malley, G. L. Timp, S. V. Moccio, *et al.*, *Appl. Phys. Lett.* **74**, 272 (1999).
159. J. J. Kopanski, J. F. Marchiando, and B. G. Rennex, *J. Vac. Sci. Technol. B* **18**, 409 (2000).
160. R. N. Kleiman, M. L. O'Malley, F. N. Baumann, *et al.*, *J. Vac. Sci. Technol. B* **18**, 2034 (2000).
161. G. H. Buh, H. J. Chung, C. K. Kim, *et al.*, *Appl. Phys. Lett.* **77**, 106 (2000).
162. D. M. Schaadt, E. J. Miller, E. T. Yu, and J. M. Redwing, *Appl. Phys. Lett.* **78**, 88 (2001).
163. K. V. Smith, X. Z. Dang, E. T. Yu, and J. M. Redwing, *J. Vac. Sci. Technol. B* **18**, 2304 (2000).

164. T. Yamamoto, Y. Suzuki, H. Sugimura, and N. Nakagiri, *Jpn. J. Appl. Phys.* **35**, 3793 (1996).
165. C. J. Kang, G. H. Buh, S. Lee, *et al.*, *Appl. Phys. Lett.* **74**, 1815 (1999).
166. M. Hammar, E. Rodriguez Messmer, M. Luzuy, *et al.*, *Appl. Phys. Lett.* **72**, 815 (1998).
167. J.-K. Leong, J. McMurray, C. C. Williams, and G. B. Stringfellow, *J. Vac. Sci. Technol. B* **14**, 3113 (1996).
168. J.-K. Leong, C. C. Williams, J. M. Olson, and S. Froyen, *Appl. Phys. Lett.* **69**, 4081 (1996).
169. P. J. Hansen, Y. E. Strausser, A. N. Erickson, *et al.*, *Appl. Phys. Lett.* **72**, 2247 (1998).
170. H. Yamamoto, T. Takahashi, and I. Kamiya, *Appl. Phys. Lett.* **77**, 1994 (2000).
171. O. Bowallius and S. Anand, *Mater. Sci. Semicond. Process.* **4**, 81 (2001).
172. T. Hochwitz, A. K. Henning, Ch. Levey, *et al.*, *J. Vac. Sci. Technol. B* **14**, 440 (1996).
173. K. Kimura, K. Kobayashi, H. Yamada, and K. Matsushige, *Appl. Surf. Sci.* **210**, 93 (2003).

*Translated by L. Man*